TECHNICAL JOURNAL

2008

University of Engineering and Technology Taxila

TECHNICAL JOURNAL

2008

**University of Engineering and Technology
Taxila**

EDITORIAL BOARD

CONTENTS

Modal and Harmonic Analysis of L.P. Turbine of a Small Turbo-Fan Engine using Finite Element Method

H. A. Khawaja[1] and A. M. Khan[2]

Abstract

History speaks of many accidents which occurred and whose cause could not be ascertained. Later it was revealed that there is a phenomenon of vibration called resonance which can occur in any engineering structure which has mass and elasticity. Different techniques, experimental and theoretical have been developed to analyze problems related to vibration. But in the present era computational techniques are quite common and are very reliable as far as the vibration analysis is concerned. In this work, the low pressure turbine of a small turbo-fan engine is analyzed for its vibration behavior using finite element method (FEM). The geometry of the turbine has been provided by the aero-propulsion designers, which was modeled in ANSYS®. To save computational time, the turbine has been modeled as a 2-D plate type of structure utilizing 4-noded Shell 63 element of ANSYS®. Constraints were applied keeping in view the actual operating conditions. The turbine was modeled with more than one FE meshes. Mesh sensitivity analysis was carried out to ensure the quality of results. Modal analysis was conducted to calculate few initial natural frequencies. Results were studied in depth against operating frequency of the turbine. After carrying out the modal analysis, harmonic analysis was done to see the response of the turbine under dynamic loading. Nature and cause of the dynamic loading is also discussed in relation to dynamic behavior. It was observed that turbine is safe in its entire range of operation as far as phenomenon of resonance is concerned. Also it was observed that maximum harmonic response of the turbine on the application of dynamic loading is far lesser than its failure limit within specified operating range.

Keywords: Modal analysis, Harmonic analysis, FRF, Turbo fan engine, Resonance

Introduction

Vibration deals with the oscillatory motion of dynamic systems. A dynamic system is a combination of matter possessing mass and whose parts are capable of relative motion. All bodies possessing mass and elasticity are capable of vibrating at specific natural frequency. The phenomenon of resonance occurs if the natural frequency of structural system matches with the frequency of dynamic loading, which may result in failure of structure. In order to avoid such failure, the study of vibrational behavior of the system is essential and in fact, absolutely necessary.

Today computational power is much larger, more reliable, and relatively cheap and as most technological related setups have access to computers, the popularity of using numerical methods is an ever increasing phenomenon. Especially FE methods are being used at large extent for structural analysis. V.Ramamurti, D. A. Subramani and K. Sridhara [1] have analyzed vibration using FE methods. Also A. M. Khan, Malik Nazir Ahmed and Shehnaz Mushtaq [2] have used FE methods for stress analysis. Other than discussed, ANSYS® Inc. has verified FE methods by solving several problems and provided number of verification manuals related to static, modal, harmonic, etc analyses [6, 7].

The primary objective of our study is to carry out the vibration analysis of L.P. turbine. This turbine is subjected to high RPM which may cause undesirable vibration. The ultimate goal in the study of vibration is to determine its effect on the performance and safety of the system under consideration.

In this work, FE method was used for the vibration analysis of turbine using commercially available software ANSYS®. CAD model was developed as per the design specification provided by the aero-propulsion experts. Material for turbine was specified as Inconel 718 [8], whose mechanical properties were taken for analysis.

[1,2] Department of Aerospace Engineering, College of Aeronautical Engineering, NUST .

Finite Element Modeling and Applied Constraints

For this work, the geometry was built in Pro-E CAD software, which can be seen in Figure 1. This geometry was imported into ANSYS® modeling environment by converting CAD file into IGES format. Additional trimming was done in ANSYS® modeling environment. To save computational time, the turbine has been modeled as a 2-D plate type of structure. This was meshed with 4-noded Shell 63 element of ANSYS®. Cyclic symmetry was utilized to decrease the computational requirement for analysis.
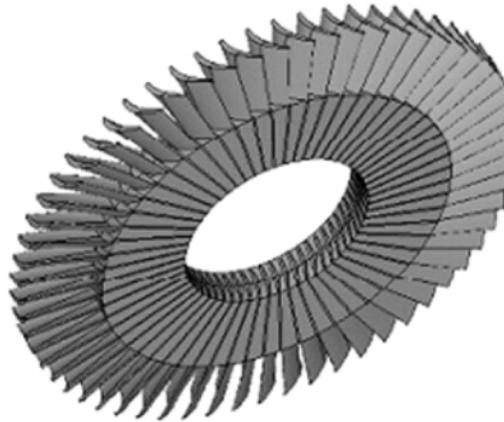
Figure 1: CAD Model of Turbine

Complete turbine was divided into 53 cyclic symmetric sectors according to the number of blades in the turbine. Figure 2 shows the finite element mesh of a single sector. For the purpose of analysis, constraint equations are developed to correctly simulate the turbine disc and blade joints. After that one sector is solved and result can be expanded to the complete turbine.
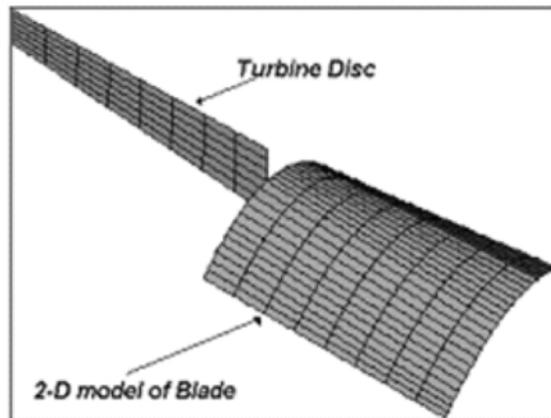
Figure 2: Finite Element of Turbine Sector

In order to gain confidence on the results, turbine was modeled with more than one mesh. Mesh sensitivity analysis were then carried out to have a mesh with an optimum number of nodes and elements. An optimized mesh should be capable of giving accurate results with minimum utilization of computational resources.

As far as boundary conditions are concerned, all nodes at turbine shaft-linkage as shown in Fig. 3 were constraint in all DOFs (Degree of Freedoms). Node coupling was used to connect nodes at blade-hub Joint (see Fig. 4). Both analyses were carried out using linear-elastic material model.
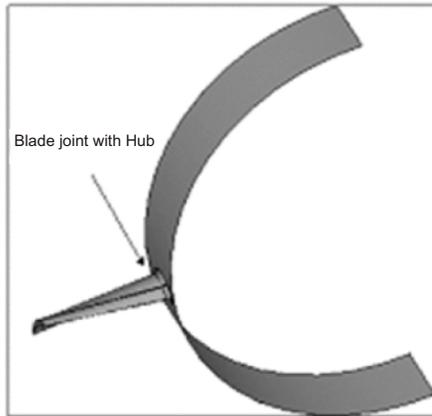
Figure 3: Illustration of Blade Hub Joint (Single Blade)
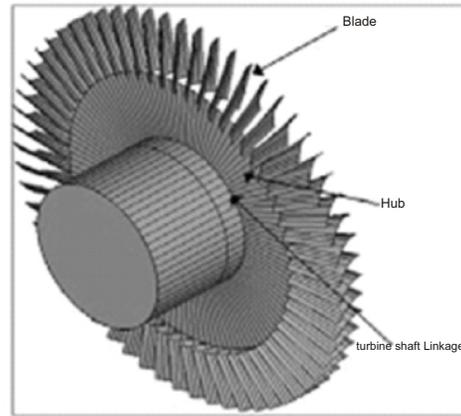
Figure 4: Illustration of turbine shaft Linkage

Modal Analysis and Applied Loads

Modal analysis is used to determine the natural frequencies of a structure. The natural frequencies and mode shapes are important parameters in the design for dynamic loading conditions. Modal analyses can be performed on a pre-stressed structure, such as a spinning turbine blade. For the modal analysis of a turbine, loads and constraints were applied keeping in view the actual situation. Loads and operating conditions of turbine as per the aero-propulsion experts are specified in Table 1.

Table 1: Operating Conditions of Turbine

Maximum Presure	0.383 MPa
Maximum Temperature	944.44 K
Operating RPM (Inertia)	32200 RPM

Modal Analysis Results

First five natural frequencies were calculated for both the cases i.e. with stress stiffening on and with stress stiffening off Results of modal analysis have not been affected much because of applied loads. The comparison of both the results is given in Table 2.   We found that there is not much difference in both the results. We also observed that operating RPM of turbine is far lesser in value than first modal frequency as shown in comparison "Table 3". Mode shapes obtained for turbine are described "Table 4".

Table 2: Modal Analysis Results

Mode No.	Natural Frequencies With Stress-Stiffening Effect (Hz)	Natural Frequencies Without Stress-Stiffening Effect (Hz)	Mode Shape Nomenclature
1	2250	2248	1st Bending
2	6080	6075	2nd Bending
3	8185	8176	1st Twisting
4	10102	10095	3rd Bending
5	14886	14876	4th Bending

Table 3: Comparison of minimum modal frequency and operating RPM

Operating RPM(Hz)	First Modal RPM(Hz)
32200 (537)	135000 (2250)

Harmonic Analysis

Any sustained cyclic load will produce a sustained cyclic response (a harmonic response) in a structural system. Harmonic response analysis is used to predict the sustained dynamic behavior of the structure, thus verifying whether or not structure will successfully overcome resonance, fatigue, and other harmful effects of forced vibration.

Harmonic analyses require cyclic load data for the analysis. This load data was gathered as per the aerodynamic analyses of turbine carried out earlier by aero-propulsion experts. It was found out that pressure load is the only load which is cyclic in nature under steady state operation. Reason for this variation is the existence of wake due to the presence of nozzle guide vanes (stators) before turbine rotors. Whenever the rotor passes by a stator it has to pass in low pressure region (wake). The repetition of this low pressure region is equal to the number of stators before the turbine. Frequency of this dynamic loading is equal to product of number of stators and turbine RPM. This phenomenon is explained in Figures 5 (a) & (b). This analysis was carried out for normal and over run operation (32200 & 38000) X 31 RPM or 16636 to 19633 Hz. The number of stators before turbine rotors is 31.

Harmonic Analysis Results

Harmonic analysis results are in the form of a graph commonly known as FRF (frequency response function). FRF for this analysis is shown in Fig. 6.   This FRF is specific to the node at the trailing edge of the tip of the turbine blade, which showed the most aggressive behavior to cyclic loading. Other nodes were also analyzed, as they showed similar response but value of displacement was lesser compare to selected node, so shown FRF is associated to tip trailing edge node. Location of specific node is shown in Fig.7.

Table 4 Turbine Mode Shapes with Description

(a) Rotor position according to stator location

(b) Rotor in the wake of stator location
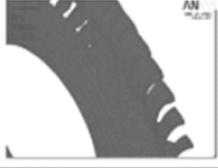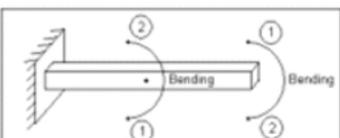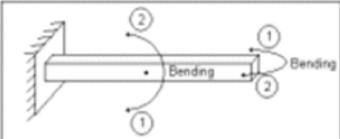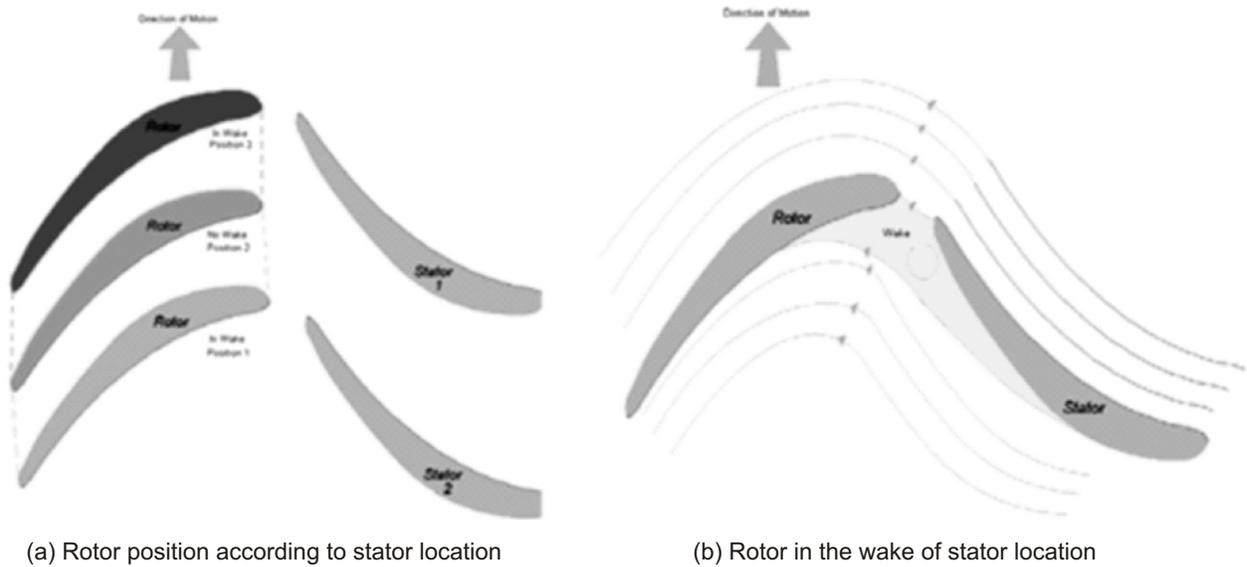
Figure 5: Illustration of pressure variation on rotor blades due to wake of stators blade

Value of the maximum displacement indicated by FRF is very small as compared to the value of maximum displacement calculated using static analyses of turbine, under which turbine blade is safe for operation. The comparison of displacements at maximum RPM, obtained through analyses is shown "Table 5".
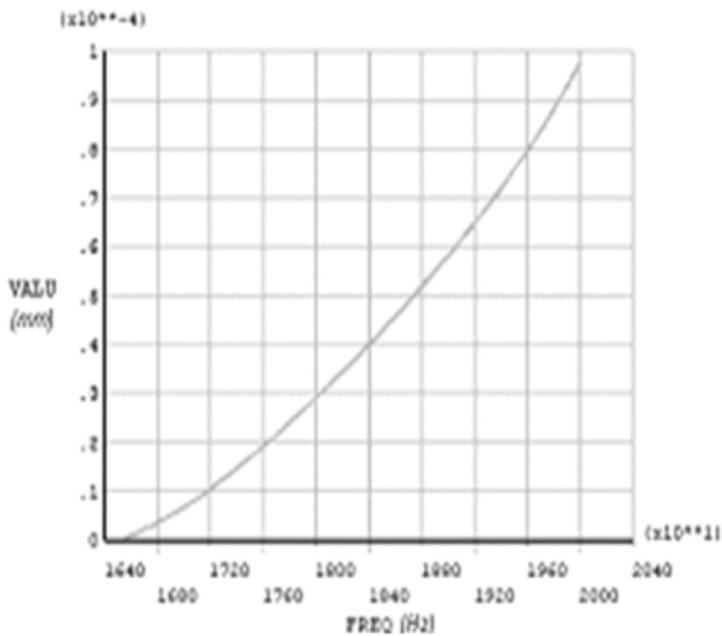
Figure 6: FRF (Frequency Response Function)

Figure 7: Node at Trailing Edge of the Tip of the Turbine Blade

Table 5: Comparison of value of maximum displacements at 19633Hz

Maximum Displacement (Harmonic Analysis)	Maximum Displacement (Static Analysis)
0.0001 mm	0.40 mm

Conclusion

Natural frequencies as per the modal analysis are shown "Table 2". This turbine has to operate at 32200 RPM or 536 Hz as per the design specification provided by aero-propulsion experts. The evaluation shows that the first natural frequency is far higher than maximum operating frequency, this gives clear indication that turbine is safe against resonance phenomenon. Also harmonic response within specified range is also acceptable, as maximum value of displacement is far lesser than static displacement. Also FRF indicates no chances of the occurrence of resonance within this range.

Acknowledgment

References

[1]   V. Ramamurti, D. A. Subramani and K. Sridhara (1998) Mach. Theory 30, 619-628.

[2]   Abdul Munem Khan, Malik Nazir Ahmed and Shehnaz Mushtaq (2006) J. of Eng. & App. Sc. 25, 47-55.

[3]   Francis S. Tse, Ivan E. Morse, Rolland T. Hinkle (1978) Mechanical Vibration 2nd Edition, Allyn and Bacon, Inc., Boston, Massachusettes.

[4]   Ernest E. Sechler (1963) Elasticity In Engineering, John Wiley and Sons, Inc., New York, USA.

[5]   ANSYS® Inc. Version 9.0, Multiphysics.

[6]   ANSYS® Inc. Version 9.0, Theory Reference, 1 Structure, 2 Modal Analysis, 3 Harmonic Analysis. 2

[7]   ANSYS® Inc. Release 9.0 Documentation, 1Structural Analysis Guide, and Verification Manuals.

[8]   Material Handbook of High Performance Alloys, Special Metals Corp., (2001).

Finite Element Approach For the Development of Mathematical Model for the Fatigue Life of Fiber-Reinforced Composite Materials

M. Nadeem Tahir[1] and Sagheer Ahmed[2]

Abstract

Preventing failure of mechanical systems has been an important issue in engineering design ever since the early stages of the industrial era. For standard design purposes the yield limit is often used as a failure criterion, which means that the component will never undergo permanent deformation under design loads. However, when safety and reliability are critical (e.g., in nuclear installations) or when the added weight and cost of over dimensioning cannot be tolerated (aircraft), more accurate predictions are needed for the onset of failure, as well as of the fracture process itself (crack paths, residual strength, remaining service life, etc.).

Today, a lot of research is dedicated to the fatigue behavior of fiber-reinforced composite materials, due to their increasing use in all sorts of applications especially in the field of aerospace, naval and automotive. Composite materials are inhomogeneous and anisotropic, and their behavior is more complicated than that of homogenous and isotropic materials such as metals. The principal objective of the research reported in this paper was to develop mathematically consistent continuum damage formulation, which can realistically describe fatigue processes. A key issue in the development of continuum damage and other fatigue models is their ability to correctly describe the localized deformations, which are characteristics of fatigue problems. If this issue is not properly addressed, the damage process, which presents the initiation and growth of cracks, tends to localize in a vanishing volume. A perfectly brittle response is then obtained, even if the constitutive relations show a gradual loss of strength. The material constants used in the model are determined using the experimental data. This model can be used to predict the fatigue life of an E-glass/vinyl ester polymer composite at any applied load.

Keywords: Finite Element Methods, Fatigue Life, Fiber-Reinforced Composite Materials, Continuum Damage Mechanics

Introduction

Composite materials are a combination of two or more chemically different materials with a distinct interface between them. The constituent materials maintain their separate identities (at least microscopically) in the composite, yet their combination produces properties and characteristics that are different from those of the constituents. Fiber-reinforced composite materials for structural applications are often made in the form of a thin layer called Lamina. A lamina is a macro unit of material whose material properties are determined through appropriate laboratory tests. Stacking the layers to achieve desired overall strength and stiffness then forms structural elements, such as beams, bars or plates. The development of composites reinforced with boron, carbon or other advanced fibers started in the aerospace industry nearly 55 years ago. Since the 1950s, NASA, the U.S. Department of Defense, and governmental agencies in the United Kingdom and other countries have supported not only research also the development, design, full scale testing, and certification of fiber reinforced polymers and their application in aircraft, helicopters, and space vehicles [1]. Since the 1995, Pakistani governmental and private agencies have been involved in the research and development of composite materials especially in the field of automobile, armors, and missiles. The most distinct exponent of continuum approaches towards fracture is continuum damage mechanics. It introduces a set of field variables (damage variables), which explicitly describe the local loss of material integrity. The notion of a continuous representation of z intrinsically discontinuous - material damage stems from the work of Kachanov [2] on tertiary creep and was further developed by Rabotnov [3]. But it was not before the mid-1970s that it was realized that the theory could be used to describe not only the formation, but also the growth of macroscopic cracks [4]. A crack is then represented by that part of the material domain in which the damage has become critical, i.e.,

[1,2] Department of Mechanical Engineering, Faculty of Mechanical & Aeronautical Engineering, University of Engineering & Technology Taxila, Pakistan.

where the material cannot sustain stress anymore. Redistribution of stresses results in the concentration of deformation and damage growth in a relatively small region in front of the crack tip. It is the growth of damage in this process zone which determines in which Fracture" which is sometimes used for this type of crack modeling.

Elasticity Based Damage

The well known classical stress-strain relation of elasticity based damage mechanics reads in its most general form :

$$\sigma_{ij} = (1 - D)C_{ijkl}\varepsilon_{kl} \tag{1}$$

Where the strain tensor is

$$\varepsilon_{kl} = \frac{1}{2}\left(\frac{\partial u_k}{\partial x_l} + \frac{\partial u_l}{\partial x_k}\right) \tag{2}$$

The elastic constants Cijkl are given by

$$C_{ijkl} = \lambda\delta_{ij}\delta_{kl} + \mu(\delta_{ik}\delta_{jl} + \delta_{il}\delta_{jk}) \tag{3}$$

Where δ the Kronecker delta and λ and μ Lame's constants. The latter can be expressed in terms of Young's modulus E and Poisson's ratio υ according to

$$\lambda = \frac{Ev}{(1+v)(1-2v)}, \qquad \mu = \frac{E}{2(1+v)} \tag{4}$$

By substituting equations (1) and (2) into the standard equilibrium equation

$$\frac{\partial \sigma_{ij}}{\partial x_i} = 0 \tag{5}$$

And solving we get

$$(1-D)C_{ijkl}\frac{\partial^2 u_k}{\partial x_i \partial x_l} - \frac{\partial D}{\partial x_i}C_{ijkl}\frac{\partial u_k}{\partial x_l} = 0 \tag{6}$$

When the appropriate conditions are satisfied, the growth of damage is governed by an evolution law, which reads in its most general form

$$\dot{D} = g(D,\tilde{\varepsilon})\dot{\tilde{\varepsilon}} \tag{7}$$

Integrating equation (7) over one loading cycle and approximating the growth of damage within This cycle, results in a relation of the form [6] [7]:

$$\frac{\partial D}{\partial N} = G(D,\varepsilon_a) \tag{8}$$

For the evolution function g (D, ε) an expression that is slightly different from that of Paas [6] is used here:

$$g(D,\tilde{\varepsilon}) = Ce^{\alpha D}\varepsilon^{-\beta} \tag{9}$$

With C, α and β material parameters after substitution of eq. (9), relation (8) can then be integrated over N cycles, yielding [8]:

$$D = -\frac{1}{\alpha}\ln(1 - \frac{2\alpha C}{\beta+1}\varepsilon_a^{\beta+1}N) \tag{10}$$

By putting D =1 in relation (3.12) and solving for N gives the following relation for Nf the Fatigue life:

$$N_f = \frac{\beta+1}{2\alpha C}(1-e^{-\alpha})\varepsilon_a^{-(\beta+1)} \qquad (11)$$

In terms of relative number of cycles N/Nf

$$D = -\frac{1}{\alpha}\ln\left(1-(1-e^{-\alpha})\frac{N}{N_f}\right) \qquad (12)$$

This relation has been plotted in Figure 1 for several values of the parameter α. The effect of variation of this parameter is quite clear: a higher value of α result in an initially slower accumulation of damage, but a higher growth rate towards the end of the fatigue life.
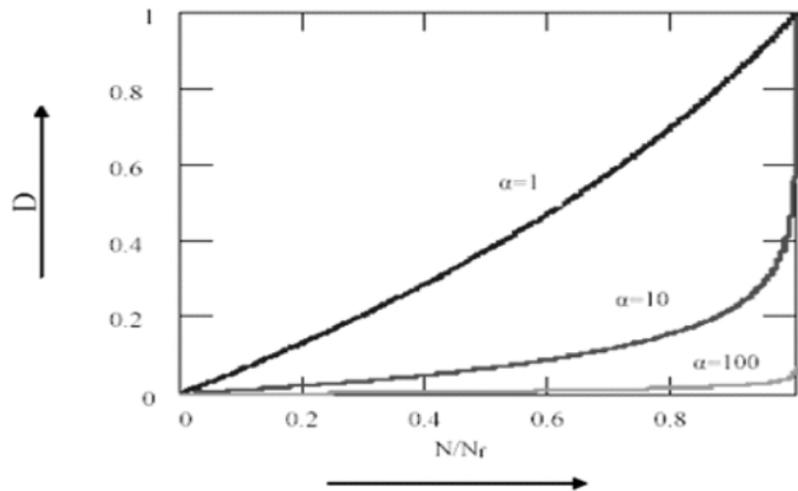
Figure 1: Damage Variable as a function of the relative number of cycles.

The incremental damage per loading cycle, dD/dN, as a function of cumulative damage, D, which may be derived from Figure 2, may be expressed in either of the following two functions:

$$\frac{dD}{dN} = \frac{C_1}{D^{n_1}} + \frac{C_2}{(1-D)^{n_2}} \qquad (13)$$

$$\frac{dD}{dN} = B_1 e^{-n_1 D} + B_2 e^{n_2 D} \qquad (14)$$

Where N is the number of loading cycles, and C_1, C_2, B_1, B_2, n_1 and n_2 are constants with n_1, $n_2 > 1$

However, experimental data on the cumulative damage, D, as a function of the number of loading cycles, N, for most of the composites do not show any initial strength degradation until the number of loading cycles exceeds 1000. Further, the initial damage does not reveal any evidence of an abrupt growth phenomenon. Instead, the normalized modulus data shows smooth, gradual decrease from the undamaged state. Therefore, for simplicity, C1 is negligible in comparison with C2. Consequently, the damage rate per loading cycle may be expressed by the following function:

$$\frac{dD}{dN} = \frac{C}{(1-D)^n} \tag{15}$$

$$\frac{dD}{dN} = Be^{nD} \tag{16}$$

Where B, C and n are again material constants. In Figure 2, the curves represented by Eq. (15) and Eq. (16) are compared with B = C = 1. From this figure, Eq. (15) appears to better represent the sudden rupture of the composite material as D approaches unity. Therefore, Eq. (15) will be expanded to describe the fatigue process for composites materials.

Besides the state of damage, the maximum stress and stress amplitude may also have substantial effects on the damage growth. Accordingly, Eq. (15) may be rewritten as:

$$\frac{dD}{dN} = C_0 \frac{(\sigma_{max}\sigma_{amp})^n}{(1-D)^n} \tag{17}$$

where

C_0, m and n are material constants,
σ_{max} is the maximum stress,
σ_{min} is the minimum stress,
σ_{amp} is the cyclic stress amplitude and is equal to (σ_{max} - σ_{min})

We can express the maximum stress and stress amplitude in normalized terms with respect to the ultimate tensile strength ($_{ult}$) and the minimum to maximum stress ratio R:

$$S_{max} = \frac{\sigma_{max}}{\sigma_{ult}} \tag{18}$$

$$S_{amp} = \frac{\sigma_{amp}}{\sigma_{ult}} = \frac{(\sigma_{max} - \sigma_{min})}{\sigma_{ult}} = \frac{\sigma_{max}}{\sigma_{ult}}(1 - \frac{\sigma_{min}}{\sigma_{max}}) = S_{max}(1 - R) \tag{19}$$

Substituting for S_{max} and S_{amp} in Eq. (17) and then simplifying, the equation becomes

$$\frac{dD}{dN} = C\frac{(S_{max}^2(1-R))^m}{(1-D)^n} \tag{20}$$

Integrating Eq. (20) and substituting the initial condition, i.e., D = 0 when N = 0, we obtain:

$$\frac{1}{n+1} - \frac{(1-D)^{n+1}}{n+1} = C(S_{max}^2(1-R))^m N \tag{21}$$

When the number of loading cycles approaches the maximum number of cycles N_f, D approaches 1. Under this condition, Eq. (21) becomes:

$$\frac{1}{n+1} = C(S_{max}^2(1-R))^m N_f \tag{22}$$

Eq. (22) is equivalent to the power formula often seen in the literature as:

$$\sigma_{max}^A N_f = cons\tan t \tag{23}$$

Which can also be expressed as?

$$\log \sigma_{max} = -\frac{1}{A} \log N_f + cons \tan t \qquad (24)$$

In the model validation section, this equation will be compared with the following expression:

$$\sigma_{max} = m \log N_f + cons \tan t \qquad (25)$$

Which is commonly used for characterizing fatigue life, Nf, of materials.

Experimental Work

The specimens used for this study were obtained from a pultruded vinyl ester/E-glass fiber composite being used in the construction of composite bridges in the world. The fiber volume fraction was approximately 28 % to 30 %, as determined by combustion of the matrix. The specimen is shown as:

The quasi-static properties of the composite material were obtained on a screw driven Instron tensile testing machine. Strain data was recorded with an extensometer, and transverse and axial strains were obtained using CEA-13-125WT-350 strain gauges. Specimens were tested at a displacement rate of 2.5 mm/min. The tests were performed according to ASTM D 3039. The following properties were obtained.
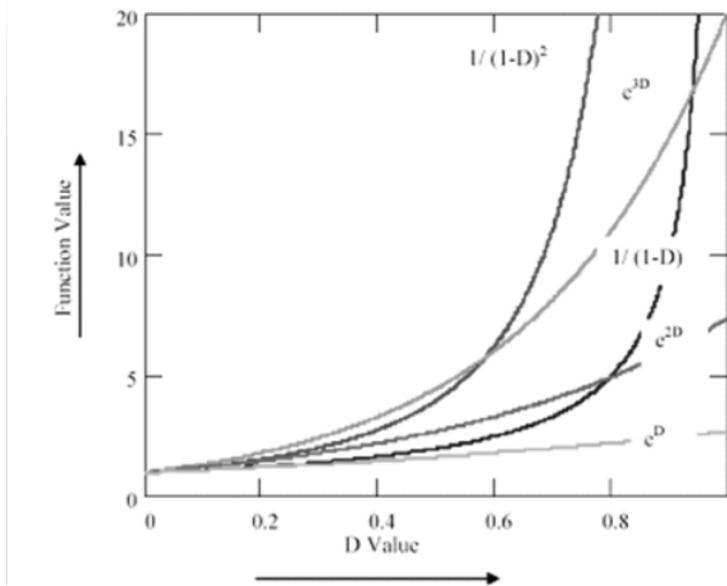
Figure 2: Comparison between damage growth as a function of exponential damage and inverse exponential damage for different values of n.
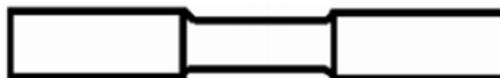

Figure 3: Specimen for Fatigue testing

Fatigue experiments were conducted under the following loading and environmental conditions:

1)   Loading mode: Rotating Bending (Tension and compression)
2)   R (minimum stress to maximum stress ratio): 0.1
3)   Test frequency: 2860 rpm
4)   Test temperature: Room temperature

All fatigue specimens were tested using the R. R. Moore Rotating Beam Fatigue Test System with the following specifications:

1) Type: FTO-20
2) Capacity: 20Kgf-m
3) Make: Tokyo testing Machine Manufacturing Company (Ltd.) Tokyo Japan
4) Motor: 0.75 KW, 02 poles, 03 phase Induction Motor with 2860 rpm

Table 1: Mechanical properties of vinyl ester/E-glass fiber composite

Mechanical Properties	Mean	Std. dev.
Ultimate Tensile Strength (MPa)	212	17.9
Modulus (GPa)	15.55	0.66
Poisson's Ratio	0.31	0.03

The R. R. Moore recognized as the standard for rotating beam fatigue testing, has been serving industry faithfully over 70 years. The machine design is based on the rotating beam principle. The specimen functions as a simple beam symmetrically loaded at two points. When rotated one half revolution, the stresses in the fibers originally below the neutral axis are reversed from tension to compression and vice versa. Upon completing the revolution, the stresses are again reversed so that during one revolution the test specimen passes through a complete cycle of flexural stress (tension and compression).

The R. R. Moore machine can be equipped to test either straight shank or tapered-end specimens. The standard specimen length is 250mm with gauge length and diameter 70mm and 15mm respectively. Straight shank specimens are held in place using precision specimen collets. Tapered end specimens are machined to match the tapers within the spindles of the machine and held in place using threaded drawbars.

Table 2: Fatigue test results for vinyl ester/E-glass fiber composite material

% of UTS	Specimen Set 1	Specimen Set 2	Specimen Set 3
80	516	434	274
70	986	693	839
60	5575	2258	1225
50	4807	4372	3470
45	24135	1000000*	1000000*
40	1000000*	1000000*	1000000*

Stress is applied to the specimen by direct application of dead weights to ensure precise loading.

Three sets of specimens (Total 18 samples) were tested at each stress level. The fatigue test data is tabulated in the table.

Model Validation

Figure 4 displays the predicted S-N curve and experimental fatigue data for the vinyl ester composite. In this figure, the normalized stress is plotted against the number of cycles in semi log scale. The normalized values were obtained by dividing the maximum applied stress by its respective ultimate strength at respective loading condition. A value of the square of correlation coefficient (r^2) between the experimental normalized stress and the number of cycles at failure is 0.8301.The square of the linear correlation coefficient quantitatively indicates the linear correspondence between two variables. An r^2 value of 1.0 means a perfect linear relationship between the two quantities; a value less than 1.0 means a less good fit.

Based on this r^2 value the equation 2.28 which is equivalent to can be used to predict the fatigue life of polymer composites used in this study.
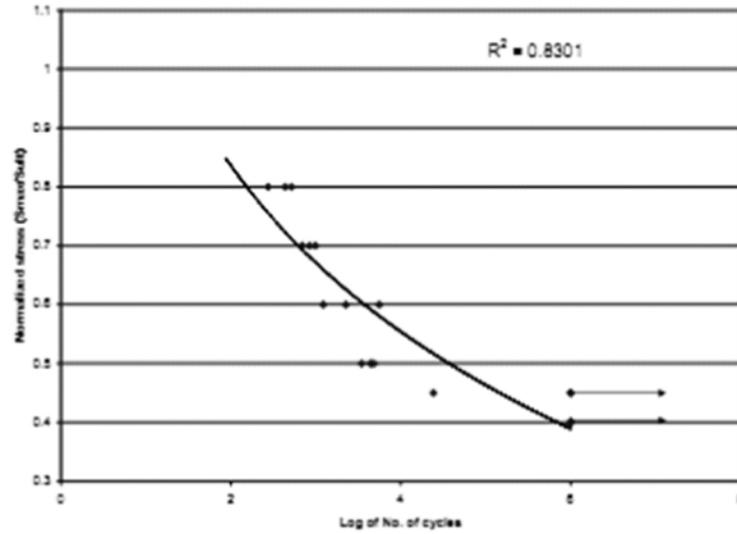
Figure 4: Predicted S-N Curve and experimental fatigue data in semi log scale

In order to determine the value of the material constant m, the Eq. (22) is rewritten into a simple linear form (y = a + bx):

$$\log(S_{max}) = -\frac{1}{2m}\log\left[(n+1)(C(1-R)^m)\right] - \frac{1}{2m}\log N_f \qquad (26)$$

$$= \frac{1}{2m}\log\frac{1}{(n+1)(C(1-R)^m)} - \frac{1}{2m}\log N_f \qquad (27)$$

Such that

$$a = \frac{1}{2m}\log\frac{1}{(n+1)(C(1-R)^m)} \qquad (28)$$

and

$$b = -\frac{1}{2m} \qquad (29)$$

Values of "a" and "b" are determined from the experimental curve as:
 a = -0.4071   and   b = 1.1184

By putting the value of "b" into Eq. (29) we get
m = 1.23

When "a" and "b" values are substituted into Eq. (26) we get the S-N curve which may be expressed as:

$$(S_{max})^{11.45} N_f = 7.16 \qquad (30)$$

This equation now can be used to find the fatigue life of vinyl ester/E-glass fiber composite materials.

Conclusion

The principal objective of the research reported in this paper was to develop mathematically consistent continuum damage formulation, which can realistically describe fatigue processes. A key issue in the development of continuum damage and other fatigue models is their ability to correctly describe the localized deformations, which are characteristics of fatigue problems. If this issue is not properly addressed, the damage process, which presents the initiation and growth of cracks, tends to localize in a vanishing volume. A perfectly brittle response is then obtained, even if the constitutive relations show a gradual loss of strength.

The model is validated by plotting the normalized stress against the number of cycles in semi log scale. A value of the square of correlation coefficient (r2) between the experimental normalized stress and the number of cycles at failure is 0.8301. The square of the linear correlation coefficient quantitatively indicates the linear correspondence between two variables. An r2 value of 1.0 means a perfect linear relationship between the two quantities; a value less than 1.0 means a less good fit. The material constants used in the model are determined using the experimental data. This model can be used to predict the fatigue life of an E-glass/vinyl ester polymer composite at any applied load.

References

[1]   P. K. Mallick, Composite Engineering Handbook, Marcel Dekker Inc., New York, 1997.

[2]   Kachanov, L. M., On the time to failure under creep conditions, Izv. Akad. Nauk. SSSR Otd. Tekhn. Nauk,. 8, 26-31, 1958.

[3]   Rabotnov, Y. N., Creep Problems in Structural Members, North-Holland, Amsterdam, 1969.

[4]   Hayhurst, D. R., Dimmer, P. R., and Chernuka, M. W., Estimates of the Creep Rupture Lifetime of Structures using the Finite Element Method, J. Mech. Phys. Solids, 23, 335-355, 1975.

[5]   Van Paepegem, W. and Degrieck, J., Fatigue Damage Modeling of Fiber-Reinforced Composite Materials: Review, Applied Mechanics Review, 54(4), 279-300, 2001.

[6]   Lemaitre, J. and Chaboche, J. L., Mechanics of Solid Materials, Cambridge University Press, Cambridge, 1990.

[7]   Pass, M. H. J. W., Continuum damage mechanics with an application to fatigue. PhD thesis, Eindhoven University of Technology, Eindhoven, The Netherlands, 1990.

[8]   Peerlings, R. H. J., Enhanced Damage Modeling for Fracture and Fatigue, PhD Thesis, Eindhoven University of Technology, Eindhoven, The Netherlands, 1999.

[9]   Tinh Nguyen, Hai Tang, A Model for Predicting the Fatigue Life of Fiber-Reinforced.

[10]   Polymeric Composites in Offshore Applications, NIST Technical note 1434, USA, 2000.

Numerical Simulation of Arc Welding Investigation of various Process and Heat Source Parameters

M. Afzaal Malik [1], M. Ejaz Qureshi [2] and Naeem Ullah Dar [3]

Abstract

The present study describes a combination of numerical simulation and experimental validation to study the temperature distribution and prediction of fusion zone (fz) and heat affected zone (haz) in gas tungsten arc welding of low carbon steel. Welding experiments are carried out on weld coupons of 3 mm thick sheet metals of 150 x 50 mm with a 2 mm square gap between them. Simulation of the entire process is accomplished by using authors written subroutines in ansys® 10.0, general purpose finite element software. The primary objective of the present study was to develop computationally efficient numerical simulation technique with in the commercially available finite element software(s) domain, for the accurate prediction of the temperature history, size of fusion and heat affected zones of the weldments. Additionally the effects of varying various significant welding and geometric parameters on the response of the weldments are also investigated with the anticipation to further utilization in the prediction of the welding induced imperfections like weldment distortions, residual stresses formation and the complex phenomenon of weld solidification cracking. The induction of carefully measured experimental data into the numerical simulations, showing close co-relation between the simulated and experimental investigations in the present study presents the significance of the numerical techniques developed for the precise prediction of transient thermal response of the weldments for the large scale industrial usage in nuclear, aeronautical, aerospace and marine engineering domains.

Keywords: Numerical Simulation, Arc Welding, "Quasi-Stationary" State, Gaussian Distribution, FEA

Introduction

The critical first step in predicting the weld induced imperfections like residual stresses, deformations, and weld solidifications cracking etc. is to accurately compute the Transient temperature fields during the arc welding process. This is necessary because the temperature has a first order effect on the microstructure, strain, stress and ultimately on the formation of defects in welds while they have at most a second order effect on the temperature fields [1].

The problem of distortion, residual stresses, and reduced strength of a structure in and around a welded joint are a major concern of the welding industry for decades. These problems primarily result directly from the thermal cycle caused by localized intense heat input in arc welding process [2]. Hence for the development of effective simulation strategy for weld analysis, the accurate prediction of thermal history is of key importance. Additionally the effects of various welding process and heat source parameters on the transient temperature states must be accurately known. The first major contribution in the field of weld thermal analysis is the analytical solution for a welding heat flow problem by Rosenthal which has been used worldwide to predict welding thermal history and cooling rates. The exact theory of heat flow due to a moving point source was first applied to arc welding by the author in 1935 using the experimentally established principle of a "quasi-stationary" state, that is, an observer stationed at the point source fails to notice any change in the temperature around him as the source moves on [3]. Later it was shown that Rosenthal's analysis which assumes a point, line, or plane source of heat is subject to serious error for temperatures in or near the fusion and heat-affected zones. The infinite temperature at the heat source assumed in this model and the temperature sensitivity of the material thermal properties (a temperature independent mean value is assumed) increases the error as the heat source is approached. Pavelic et al. first suggested that the heat source should be distributed [4]. He proposed a Gaussian distribution of flux deposited on the surface of the work-piece. Later, some authors have suggested that the heat should be distributed throughout the molten zone to reflect more accurately the digging action of the arc [1]. A double ellipsoid configuration of heat source was proposed by J. Goldak [1] so that the size and shape of the heat

[1,2] MED, College of Electrical and Mechanical Engineering, NUST, Rawalpindi.
[3] MED, University of Engineering & Technology, Taxila.

source can be easily changed to model both the shallow penetration arc welding processes and the deeper penetration in laser and electron beam processes. In addition, it has the versatility and flexibility to handle non-axis-symmetric cases such as strip electrodes or dissimilar metal joining. Welding stresses arising from the temperatures gradients due to the moving heat sources and deformations have close analytical relations. Due to heating and cooling, thermal stresses occur in the weld and the adjacent areas. The strains produced during the heating phase always induce plastic deformation of the metal. The stresses resulting from these strains combine and react to produce internal forces that cause a variety of welding distortions. Welding-induced residual stresses and shape-change behavior can play a very important role in the reliable design of the welded joints and welded structures. Finite element techniques have been used in the prediction of welding residual stress and distortion for more than two decades [5].

Due to the nature of the process, additional complexities are involved in the FEA of welding compared to traditional mechanics, such as temperature and history-dependent material properties, high gradients of temperature, stress and strain fields with the respect to time, large deformations in thin structures, phase transformation and creep phenomena [6]. The problem of distortion, residual stresses and reduced strength of structure in and around welded joints are a major concern of welding industry, primarily in aerospace industry where safety and economy are important issues.

Present Study

The present research work presents a transient non-linear thermal simulation of plate butt joint by arc welding processes using FE heat transfer analysis. A heat source model is presented based on the Goldak's method and MATLAB® scripts are developed in order to calculate the heat flux distributions and define a moving heat source into simulations by using FE software ANSYS® [7]. Full three-dimensional FE models are developed in ANSYS® for the simulation of complex, highly nonlinear phenomenon during the arc welding process with filler metal deposition, as it was used by many researchers [8, 9, 10] in the past to tackle the nonlinear problems with acceptable accuracy levels. The results from the developed modeling approach were verified by welding experiments on the same geometry with similar parameters in order to establish quantitative correlations between FE simulations and experiments. The transient temperature distribution and variation of the welded plates during welding process were predicted. The fusion zone and heat affected zone were also obtained. The effect of the heat source distribution, energy input and welding speed on temperature was investigated. The results showed that temperature distribution and variation in the welded plates are sensitive to the heat source distribution and welding process parameters. The work presented here would provide a basis for further investigations of welding distortions, residual stresses and weld solidification cracking phenomenon.

Finite Element Simulation Strategy

A three-dimensional finite element analysis strategy is developed to benchmark the experimental results from section 3.0. The size of the specimen plate is 150mm x 100mm x 3mm (length x width x thickness). Because of symmetry, only one half of the plate is modeled. The heat transfer analysis to simulate the GTA welding process is conducted through the author written subroutines in ANSYS®. Taking into account the weak nature of mechanical to thermal fields coupling, the first part of the sequentially coupled elastic-plastic thermo-mechanical analysis is discussed here in the present study and the effects of various heat source and welding process parameters on transient temperature distributions, boundary and shape of FZ and HAZ are presented in detail. The combined heat transfer coefficient for convection and radiation [11] is calculated and applied on all the surfaces (except the symmetry plane) as thermal boundary condition. The heat loss from the surfaces are modeled from the equations-1 and 2.

$$q = q + q \quad (1)$$

loss convection radiation

$$q = h \times A \,(\, T – T) \quad (2)$$

loss total amb

Where, A is the surface area, T is current temperature, Tamb is the ambient temperature and htotal is combined convection and radiation coefficient, given by the following equation.

$$h_{total}=[h+ \varepsilon\sigma (T+T_{amb})(T2+T_{amb})]$$

Where,

H = Thermal convection coefficient
 (8 W/m2-oK in the present study)
e = Radiation emmissivity
 σ = Stefan Boltzman constant
 (5.67 x 10-8 W/m-oK4)

On the surface of the steel under investigation in the present study, $\varepsilon = 0.51$ is used which is the average value for hot rolled steel plates. Tamb is taken as 300oK equal to the preheat temperature. The heating time along the weld path is about 52 sec with a torch speed of 3.0 mm/s, and the complete welding sequence is divided into 78 incremental equally spaced load / solution steps of 0.667 s. Stepped load option available in ANSYS® is used for effective application of thermal load during the load step. After extinguishing the arc additional 40 load steps of different lengths are used for cooling of the weldment. The total cooling time to return to the ambient temperature of 300oC (573.15oK) is about 23 minutes from the start of the cooling phase.

Finite Element Model in the Present Study

One-half symmetric 3D FE model for the welding of coplanar plates with v-groove developed in ANSYS® is shown in Fig. 1. The element type in thermal analysis is SOLID70 (linear 8 node brick element with one degree of freedom, i.e., temperature at each node). Further details about the selected elements may be found in [7]. The finite element statistics for the model is:-

Total No. of nodes: 1246
Total No. of elements: 9000

High temperature and flux gradients are anticipated in and around the FZ and HAZ therefore a relatively fine mesh is used within a distance of 10 mm from weld line (WL). Away from the HAZ the element size increases with an increase in the distance from WL. In weld direction, the element size is kept constant equal to 2 mm. Within the anticipated HAZ dimension of 10 mm on each side of the WL in transverse direction, the element size of 1 mm is used. The element size away from weld region increases with the increase in distance. In thickness direction there are total three elements, 1 mm each to facilitate for v-groove modeling. Two tack welds on the start and end of the weld are modeled, each of which comprises of 2 elements (4 mm) in weld direction and 2 elements (2 mm) in transverse directions and 3 elements (3 mm) in thickness direction. Tack lengths positions in the FE model are in accordance with the physical weld sample.
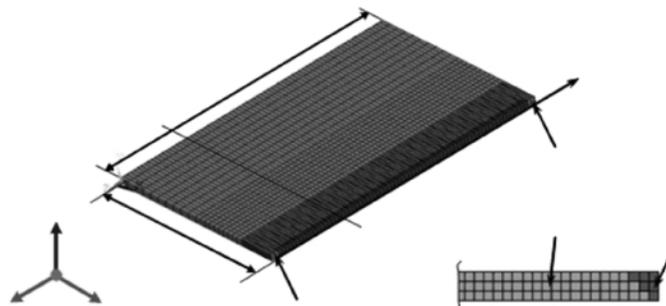

Figure 1: 3D FE model used in the present study

Moving Heat Source Model

The welding induced imperfections like residual stresses and deformations are believed to be due to highly non-uniform temperature fields generated during welding. Both the residual stresses and deformations, are highly sensitive to transient temperature distributions, which itself is a function of total heat applied and heat distribution patterns within the domain. Thus for the determination of realistic temperature profile in the target application, a very careful and accurate modeling of heat source is required. During the last four decades several developments in the heat source modeling have been reported in the literature, a very brief introduction of which can be found in [B1]. In the present study, the welded plates and filler material is modeled as solid body. The most widely acceptable double ellipsoidal heat source model, presented by Goldak et al [1] is used to present the heat generated by the welding torch. The model gives the Gaussian distribution and has excellent features of power and density distribution control in the weld pool and HAZ. The heat source distribution as shown in Fig. 2 combines two different ellipses i.e. one in the front quadrant of the heat source and the other in the rear quadrant [13].
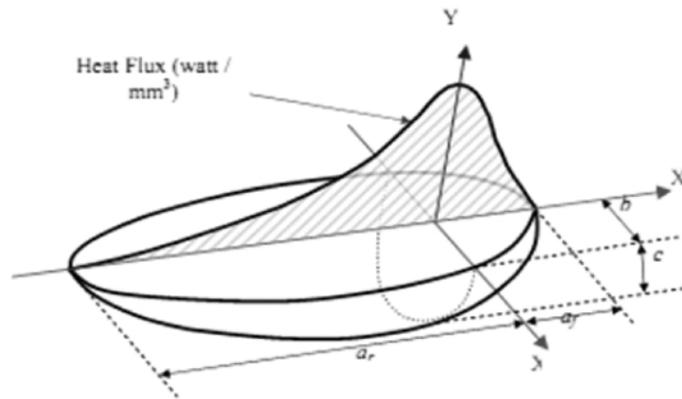

Figure 2: Heat Source model used in the present study

$$q_f = \frac{6\sqrt{3}\eta Q f_f}{\pi\sqrt{\pi}\, a_f bc}\, e^{\{-3(\frac{x^2}{a_f{}^2}+\frac{y^2}{b^2}+\frac{z^2}{c^2})\}} \qquad (3)$$

$$q_r = \frac{6\sqrt{3}\eta Q f_r}{\pi\sqrt{\pi}\, a_r bc}\, e^{\{-3(\frac{x^2}{a_r{}^2}+\frac{y^2}{b^2}+\frac{z^2}{c^2})\}} \qquad (4)$$

Where,

$Q = VI$ and $ff + fr = 2$

Q = Total heat input (watts)

V = Welding voltage (volts)

I = Welding current (amperes)

Heat Flux Distribution for FE Model

In order to simulate the welding torch movement with the specific welding speed, the calculated volumetric heat flux densities have to be assigned to specific elements around the welding areas in the FE model. In this case, the origin of the coordinate system is located at the centre of the moving arc. A user subroutine written in APDL is used to calculate the centroidal distance of elements from the moving arc centre corresponding to the arc position at any instant. Based on the FE mesh generated by the ANSYS®,

definitions of the welding process parameters and characteristics of the heat source transient heat fluxes representing the moving the distributed heat source can be calculated on specific positions in welding areas. The heat source is assumed to move through volume and calculated heat is applied to elements as volumetric heat generation. The supplementary advantage of volumetric heat generation is that the elements lying on the surface can be used for modeling of surface heat convection which otherwise require additional two dimensional surface elements to suit the purpose. The numerical values of different heat source parameters and welding process parameters used in the study are shown in Table 1 and Table 2 respectively.

Fig. 3 and Fig. 4 represent two corresponding heat flux distributions with different welding process and heat source parameters. The variation of the parameters changes the heat source distributions and magnitude, therefore influences the input of heat flux applied in the weld regions. Consequently it affects the transient temperature distributions in the fusion zone, heat affected zone and peak temperatures in the welded plates [13]

Table 1: Heat Source Parameters used			
Parameter	HSP-1	HSP-2	HSP-3
a_1	8 mm	8 mm	4 mm
a_2	20 mm	12 mm	12 mm
B	10 mm	8 mm	8 mm
C	2.5 mm	3 mm	3 mm
f_f	0.6	0.45	0.45
f_r	1.4	1.45	1.45

Table-2: Welding Process Parameters			
Parameter	WPP-1	WPP-2	WPP-3
V (volts)	175	200	300
I (amperes)	12.5	15	20
η (%)	90	90	90

Modeling of Filler Metal Deposition

Conventional quite element technique [14], which is relatively straight forward and easy to implement by utilizing the ANSYS® embed features of element birth and death, is used in the present work. The whole FE model is generated in the start however; all elements representing filler metal are deactivated by assigning them very low conductivity. During the thermal analysis all the nodes of deactivated elements (except those shared with the base metal) are also fixed at ambient temperature till the birth of the respective element. Deactivated elements are re-activated sequentially when they come under the influence of the heat source (welding torch).

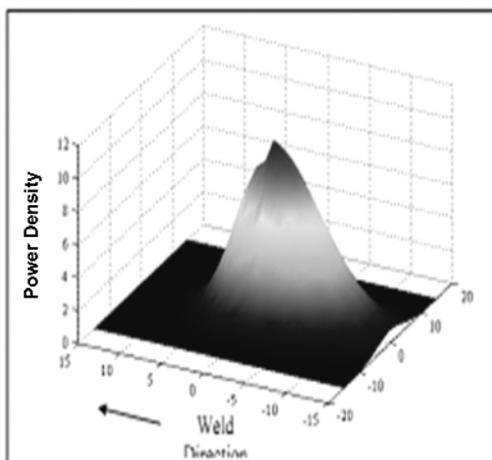
Figure 3: Power density on upper surface of the the plate with heat source parameters HSP-1 welding process parameters WPP-1
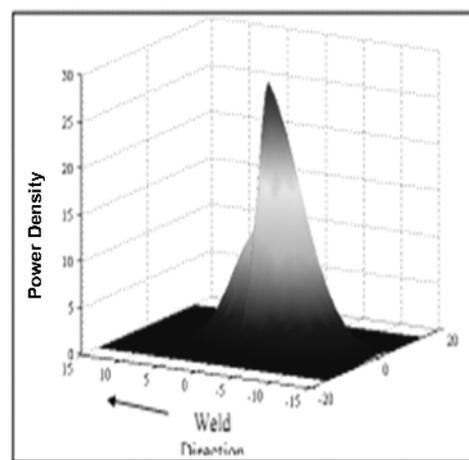
Figure 4: Power density on upper surface of plate with heat source parameters HSP-2 and welding process parameters WPP-2

Material Model

In simulation work the same material is assumed for sheet metal and filler metal. Temperature dependent material properties are taken from Karlsson and Josefson [15] as shown in Fig. 5 and Fig. 6. The melting and phase transformation temperatures of the material are taken as 1738oK and 900oK respectively. These material properties were presented for carbon-manganese steel with the composition of 0.18% C, 1.3% Mn, 0.3% Si, 0.3% Cr, 0.4% Cu.
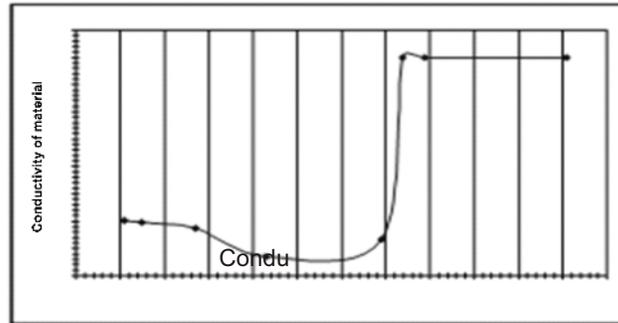

Figure 6: Temperature dependant thermal conductivity of material
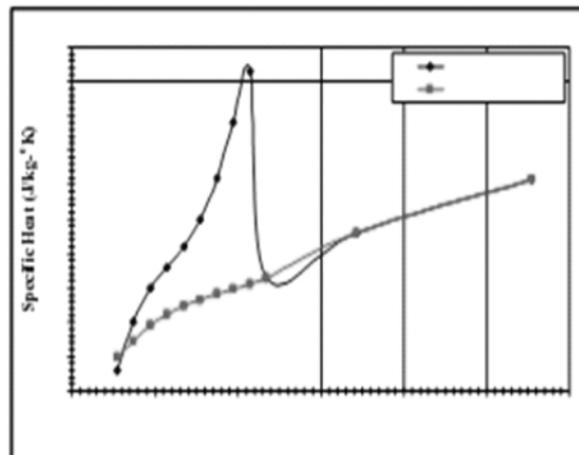

Figure 7: Temperature dependant specific heat of material

Reliability Verification for the Developed FE Model

To ensure the reliability of the finite element model developed, TIG welding experiments on two coplanar plates with similar geometric dimensions, weld parameters, and heat source parameters from the base finite element model are conducted. Commercially available mild steel with slight variations in chemical composition from the material model used in the simulation is utilized. Similar approximations were made in the past by many researchers [16, 17] with reasonable comparative results in the measured and predicted results.

Sample from the welded specimen is ground, etched, polished and the macrograph of the cross section is shown in Fig. 7 along with the superimposed cross section at similar time step from the weld experiments. The quantitative comparison of measured and predicted FZ and HAZ values are shown in Fig. 8. From Fig. 7 and Fig. 8, it is evident that predicted results agreed well with the experimentally measured FZ and HAZ. Thus, the developed models have been experimentally validated.

Scope of the Present Research

The primary objective of the present research is to address the evolution of thermal effects, fusion and heat affected zones of welded thin sheet metals of commercial mild steel by finite element methods. A

comprehensive analysis for the Gas Tungsten Arc Welding (GTAW) commonly known as Tungsten Inert Gas (TIG) welding   process for two coplanar plates with symmetry option is presented. The Scope of the present study is limited as follows:

1. Study the effects of double ellipsoidal heat source model by varying the heat source parameters. Three different set of heat source parameters are used and their effects on the evolution of temperature gradients, fusion and heat affected zones during the arc welding phenomenon are investigated. Different set of GOLDAK's double ellipsoidal heat source parameters used are shown in table-1. The corresponding distribution in power densities are shown in Fig. 3 and Fig. 4.
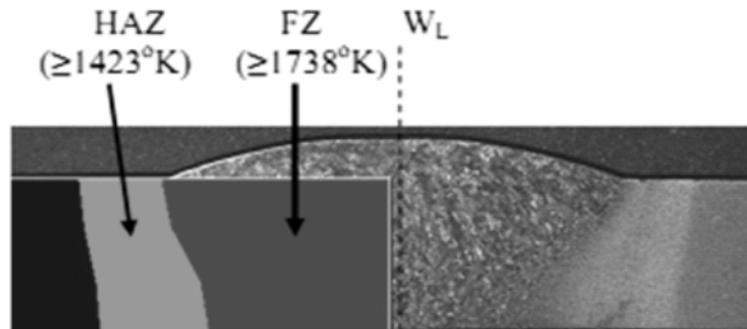

Figure 7: ISO - Parametric experimental macrograph with superimposed cross section from the simulation
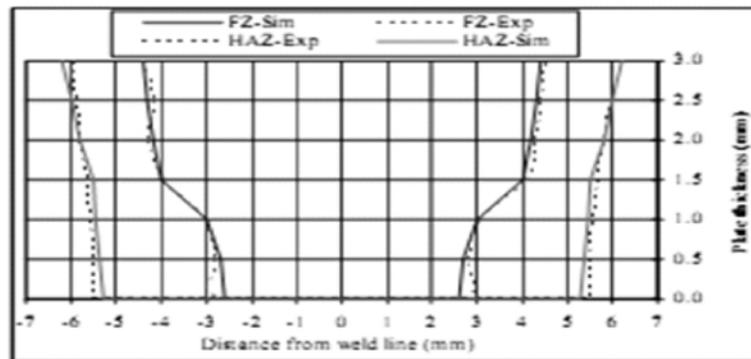

Figure 8: Quantitative comparison predicted and measured FZ and HAZ

2. Study the effects of welding process parameters on the temperature profile, fusion and heat affected zones. Three different heat inputs are used by varying the welding process parameters. The base heat input value from the experiments, govern by the arc voltage and current values of 12.5 volts and 175 amperes respectively with arc efficiency of 90%. To study the effects of variation in heat input, two additional studies with values of welding process parameters as shown in Table-2 are also used.

3. Study the effects of varying welding speed on the temperature profile, fusion and heat affected zones. Three different torch speeds are used for comparison purpose. The base value govern from the welding experiments is taken as 3 mm/sec. For comparison purpose two additional studies with torch speeds 6 mm/sec and 9 mm/sec are also conducted.

Results and Discussion

Fig. 9 shows the temperature distribution of the welded plate after 32.667 seconds and the heat source is at a distance of 98 mm from the weld start position. It is evident from the figure that the temperature around the torch reaches 2110oK suggesting melted material in the fusion zone (FZ). Next to fusion zone, the presence of higher temperatures indicates the presence of heat affect zone. A small area ahead of the heat source also shows comparatively higher temperature because of the front parameter of heat source model.

The heat input from the heat source to the weldments gradually transferred to the rest of the base plate in all directions due to conduction, convection and radiation phenomenon. Also the cooling effects can be visualized by the decreasing temperature of the weld start position where the temperature drops around 1070oK.

The evolution of temperature gradients, FZ and HAZ due to moving heat source along the weld path is obvious from Fig.9. The maximum temperature attained at the torch location along with the double ellipsoidal heat source distribution is evident. As the heat source moves away from certain point the temperature drops significantly with the passage of time. After 32.667 seconds the melted region (1738oK) of the plate reaches a temperature of 1070oK. It is believed that this high temperature heating with subsequent cooling of the weldments is the only source for the weld induced imperfections. The computed temperature histories of some selected test points throughout the welding heating and cooling sequence are shown in Fig. 10.
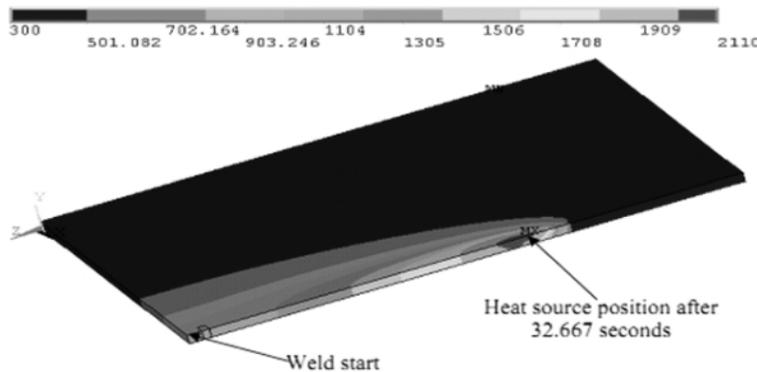

Figure 9: Temperature Distributions from FEM

The temperature distribution on the top surface (exposed directly to welding torch) of the plate transverse to welding direction with base welding process parameters (WPP-1), heat source parameter (HSP-1) and welding speed of 3 mm/sec is shown in Fig. 11.

In a similar fashion the temperature history along the weld line at different time steps with the same welding process parameters, heat source parameters and welding speed are shown in Fig. 12. Fig. 13 clarifies the temperature distribution in a reference plane taken from the simulation, when the welding torch approaches and crosses the plane. The rapid distribution of temperature in and around the fusion zone and then to the HAZ are obvious. This also shows that heat conduction is primarily responsible for most of the heat flow, whereas surface convection and radiation have little effects on FZ and HAZ boundaries.
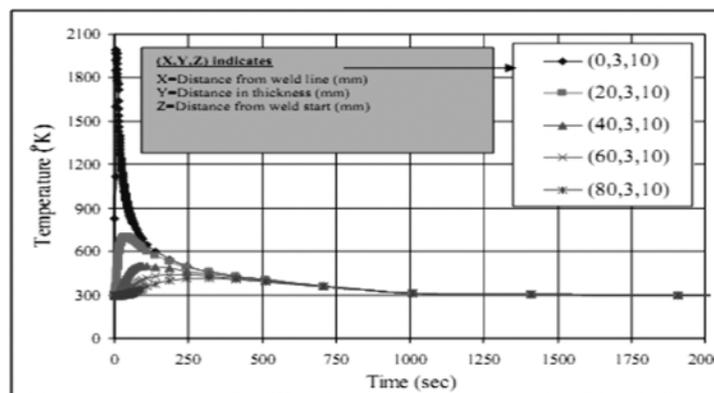

Figure 10: Temperature History of selected test points throughout the welding heating and cooling process

The effects of varying heat source parameters and welding process parameters on transient temperature distribution and evolution of FZ and HAZ are shown in Fig. 14 to Fig. 17 respectively. Heat source parameters distribution directly affects the boundaries and shape of the FZ and HAZ as shown in Fig. 14. The decrease of the FZ with increase in heat source parameters depicts the lower value of heat density applied to the surface exposed to the welding torch. The heat source parameters also affect the peak temperature considerably in FZ and HAZ as shown in Fig. 15.

The values of HSP-1 as compared to HSP-2 and HSP-3 show considerable peak temperature variations in FZ and HAZ due to significant variations in the parameters. This dictates that the transient temperature distribution is strongly sensitive to the heat source parameters.
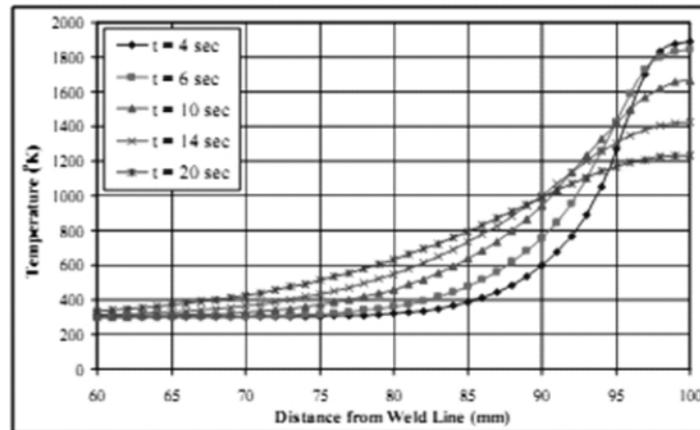
Figure 11: Temperature distributions on top surface of plate transverse to
welding direction with welding process parameters (WPP-1),
heat source parameters (HSP-1) and welding speed 3 mm/sec

Figure 12 Temperature History along the weld line,
in weld direction at selected time steps

As was anticipated, the variation in total heat energy input to the metal i.e. variation of welding process parameters primarily welding voltage, current and arc efficiency significantly affects both the boundaries (magnitude) and shape (heat distribution) of FZ and HAZ along with affecting the peak temperatures in both the zones.

Figure 13: Temperature Distribution and evolution of FZ and HAZ
in a reference plane from Simulation

Figure 14: Effects of varying heat source parameters
on shape and boundaries of FZ and HAZ

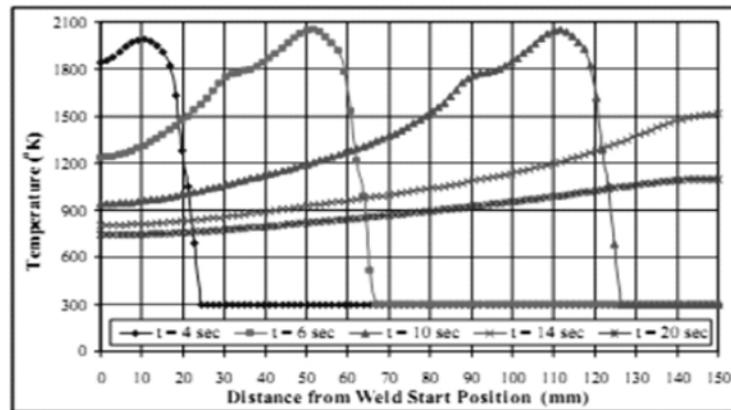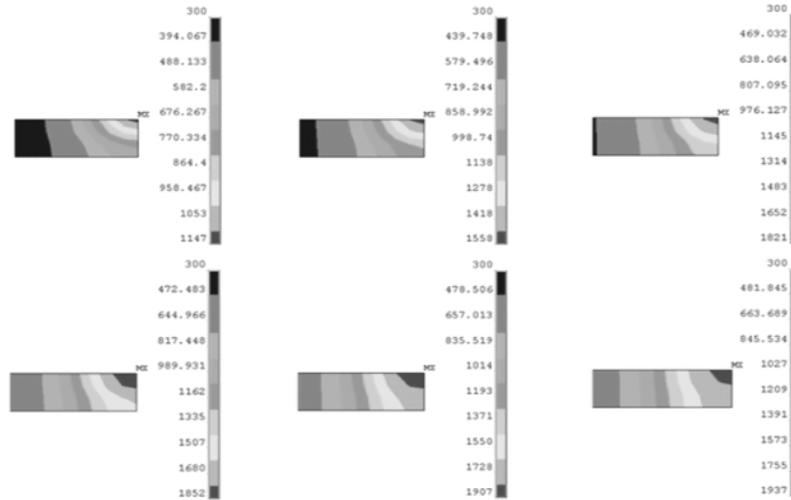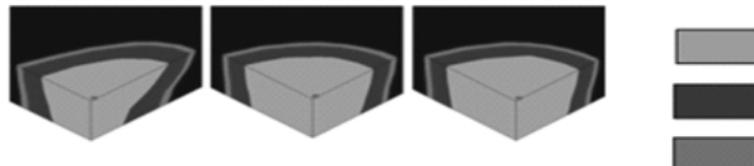As seen for heat source parameters, the effects of process parameters also have a little influence on temperature distributions on the rest of the base metal. The comparison of temperature distributions on top surface of the plate transverse to welding direction with varying welding process parameters and welding speed of 3 mm/sec is shown in Fig. 1.

With HSP-1 a gross power of 2187.5 watts is input to the upper surface of the plate. Similarly for HSP-2 and HSP-3 the heat input is 3000 watts and 6000 watts respectively. The gross heat input is used for comparison purpose only as in all the three cases the welding speed and arc efficiency are identical. Further similar heat source parameters are used to explicitly get the effects of the variable heat input. The high input in case of HSP-3 shows significantly higher peak temperature (2563oK) as compared to HSP-2 (1830oK) and HSP-1 (1720oK). An important investigation here is that the peak temperature directly depends upon the total heat input to the plate from the welding torch.

Fig. 16 shows the peak temperature achieved transverse to weld direction (section at z=90 mm) when the heat source is applied at different welding speed to the plates. It is obvious that the increase in speed will result in a shorter stay of the heat source on a specific area, dictating the lower temperatures. The same is indicated from the simulations in Fig. 16. The increase in speed only influences the peak temperatures in FZ and HAZ and has very little effects on temperature in the areas away from the heat source. Fig. 17 shows the predicted temperature profiles along the welding direction with varying welding speed. The maximum temperature from the weld start position (X=0 from Fig. 17) decreases along the weld direction for a specific time step. It is clear that welding speed significantly affects the peak temperature within the FZ and HAZ with no significant effects away from the weld line.
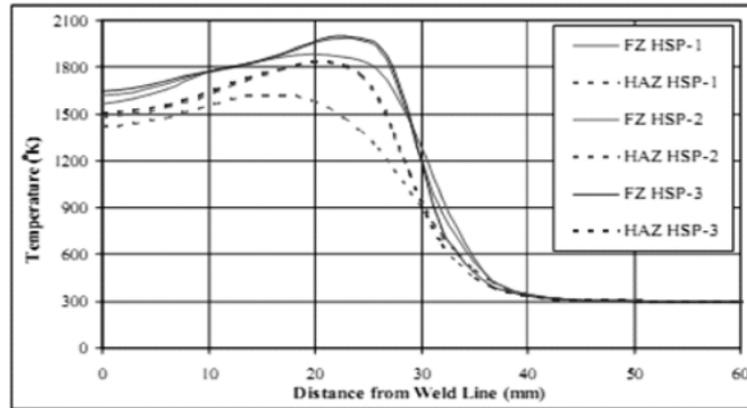
Figure 15: Effects of heat source parameters on peak temperatures in FZ and HAZ

Conclusions

A Gaussian distributed moving heat source model based on Goldak's heat source model through author written APDL subroutines and MATLAB scripts is implemented and experimentally validated for the 3D finite element simulations of arc welding process. The influence of significant welding process; and heat source parameters on transient temperature histories, shape and boundary of the FZ and HAZ is successfully demonstrated. Based on the investigations from the present research work, the following important conclusions can be drawn.
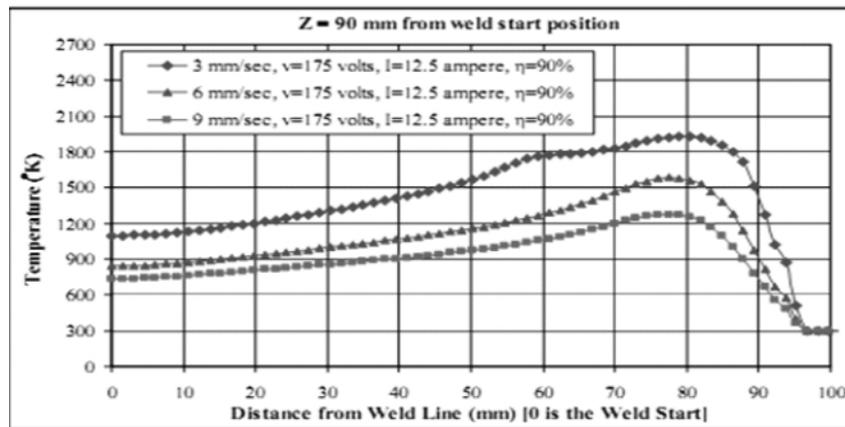
Figure 16: Effects of welding speed on peak temperature transverse to weld direction

Figure 17: Effects of welding speed on peak temperature along the weld direction

1. The results shows that welding speed, heat source parameters and the total heat input to the plates can significantly affects the peak temperatures in the FZ and HAZ. Also the shape and boundaries of FZ and HAZ are sensitive to the changes in the input parameters.

2. GOLDAK's heat source parameters distribution directly has direct affects on the Boundaries and shape of the FZ and HAZ. The heat source parameters also significantly affect the peak temperature in FZ and HAZ.

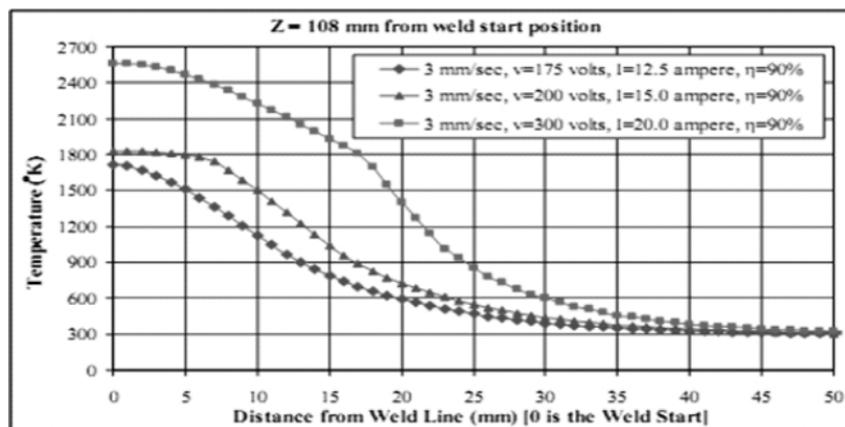3. The total heat input to the plates has obvious effects on peak temperature achieved in the FZ and HAZ. The change in temperature is approximately directly proportional to the heat input. Similarly the increase in welding speed results in decrease of the peak temperature in the FZ and HAZ.

Nomenclature

af	Length of front ellipsoidal (m)
ar	Length of rear ellipsoidal (m)
b	Width of heat source (m)
c	Depth of heat source (m)
ff	Fraction of heat in front ellipsoidal
fr	Fraction of heat in rear ellipsoidal
Qf	Power density in front ellipsoidal (W/m3)
Qr	Power density in rear ellipsoidal (W/m3)
Q	Total heat input (W)
I	Welding current (amperes)
V	Welding voltage (volts)
η	Arc efficiency (% age)

Acknowledgments

References

[1] J. Goldak, A. Chakravarti and M. Bibby: A New Element Model for Welding Heat Source. Metallurgical Transactions B, 1984. vol. 15B, pp 299-305.

[2] V. Kamala and J. A. Goldak: Error due to two dimensional approximations in heat transfer analysis of welds. Welding Research Supplement. Sep. 1993. pp 440-s-446-s.

[3] D. Rosenthal: The Theory of Moving Sources of Heat and Its Application to Metal Treatments. Trans. ASME, 1946, vol. 68, pp. 849-865.

[4] V. Pavelic, R. Tanbakuchi, O.A. Uyehara, and P.S. Myers: Welding Journal Research Supplement, 1969, vol. 48, pp 295s-305s.

[5] Computer simulation of residual stress and distortion of thick plates in multi electrode submerged arc welding, their mitigation techniques. PhD Thesis.

[6] T. D. Huang, Pingsha Dong, Lawrence. A. Decan, Dennis D. Harwig. "Residual stresses and distortions in light weight ship panel structures".

[7] ANSYS-10.0 user manual.

[8] Lu. Xiangyang, Influence of Residual Stress on Fatigue Failure of Welded Joints, PhD Thesis, North Carolina State University, 2002.

[9]   Fenggui Lu, Xinhua Tang, Hailiang Yu, and Shun Yao, Numerical simulation on interaction between TIG welding arc and weld pool, Computational MaterialsScience 35 (2006) 458-465.

[10]   Muhammad Shah Alam, Structural Integrity and Fatigue Crack Propagation Life Assessment of Welded and Weld-Repaired Structures, PhD Thesis, Louisiana State University and Agricultural and Mechanical College, Department of Mechanical Engineering, 2005.

[11]   Ihab F. Z. Fanous, Maher Y. A. Younan, Abdalla S. Wifi; Study of the Effect of Boundary Conditions on Residual Stresses in Welding using Element Birth and Element Movement Techniques, ASME Journal of Pressure Vessel Technology, vol. 125, pp. 432 - 439, 2003.

[12]   Lindgren, L.E., Finite Element Modeling and Simulation. Part 1: Increases Complexity, Journal of Thermal Stresses, vol. 24, pp. 141-192, 2001.

[13]   doi:10.1016/j.jmatprotec.2500.06.018, D. Gery, H. Long, and P. Maropoulos, Effects of welding speed, energy input, and heat source distribution on temperature variations in butt joint welding, Journal of Material Processing Technology (2005). ARTICLE IN PRESS.

[14]   Lindgren, L.E. and Hedblom, R., Modeling of Addition of Filler Material in Large Deformation Analysis of Multi-pass Welding, Communication in Numerical Methods in Engineering, vol. 17, pp. 647-657, 2001.

[15]   Karlsson, R. I. and Josefson, B. L. Three Dimensional Finite Element Analysis of Temperature and Stresses in a Single Pass Butt Welded Pipe. ASME Journal of Pressure Vessel Technology, vol. 112, pp. 76 - 84, 1990.

[16]   Muhammad Siddique., Experimental and Finite Element Investigation of Residual Stresses and Distortions in Welded Pipe Flange Joints, PhD Thesis, Ghulam Ishaq Khan Institute of Engineering Sciences and Technology, 2005.

[17]   Anderson, L. F., Residual Stresses and Deformations in Steel Structures, PhD. Thesis, Technical University of Denmark, 2000.

Fatigue Design and Validation of an ASME-Coded Pressure Vessel

R. A. Pasha[1], N. A. Choudary[2] and M.A. Nasir[3]

Abstract

Fatigue is not the most common cause of failures of pressure vessels, but designers should always take it into account due to the possible serious consequences of the failures of this type of structures and due to the fact that all pressure vessels experience some kind of fatigue loading which includes pressure fluctuations, mechanical and thermo mechanical loads.

In this work the fatigue assessment of a real size pressure vessel subjected to internal pressure fluctuations is carried out. The design of pressure vessel and evaluation of its fatigue life was done according to the rules provided in ASME boiler and pressure vessel code, section VIII, division 2. Fatigue life of designed pressure vessel was calculated by applying cyclic elastic-plastic finite element analysis. Strains and acoustic emissions were monitored during real time test. Different results obtained using the above stated procedure Designed and fabricated pressure vessel was tested experimentally. The cyclic elastic-plastic FEA proved very useful tool for predicting fatigue lives of critical areas of pressure vessel. Moreover experimental results were quite in favor of the numerical results. It was concluded that cyclic elastic-plastic FEA technique should be used in conjunction of ASME boiler and pressure vessel code, for the fatigue life evaluation of the pressure vessels especially those in which yielding of material may occur at some localized areas.

Keywords: Fatigue, ASME-BPV Code, Pressure Fluctuations, FEA, S-N Curve.

Introduction

The ASME boiler and pressure vessel code provides a fatigue evaluation procedure which is based on a comparison of peak stresses with strain cycling fatigue data. The strain cycling fatigue data is represented by the design fatigue strength curves. In these curves the alternating stress is plotted against the number of cycles. This stress is calculated on the assumption of elastic behavior but it does not represent a real stress when the elastic range is exceeded. The stress, on a gross scale, is elastic, but the metal deforms plastically at some localized areas. Such plastically deformed areas are constrained by the surrounding elastic material, thus the overall structural response remains elastic. However the plastically deformed regions are potential sites for crack initiation resulting in a finite life of a component. At higher stresses the fatigue life is progressively decreased, but the gross plastic deformation makes interpretation difficult in terms of stress.

Fatigue design and fatigue related problems have been identified as a major area of concern in a 1996 survey conducted by the newly formed European Pressure Equipment Research Council [1].Chang T. Y worked on elastic-plastic deformation of cylindrical pressure vessels under cyclic pressure. He used a numerical procedure based on the finite element method and incremental solution approach for analyzing cylindrical pressure vessels deformed in the state of generalized plane strain [2]. This present task was performed using elastic-plastic finite element calculations applying sub modeling techniques. This technique allows the structural details modeling using solid elements, applying boundary conditions imported from a global model based on shell elements.

Design and Fatigue Evaluation by ASME Code

Pressure vessel is designed according to the rules of ASME boiler and pressure vessel code, section VIII, division 2 [3]. Then the fatigue lives of individual parts of the pressure vessel are evaluated according to the mandatory appendix 5. Three main parts of the pressure vessel i.e/ shell, flat head and nozzle were fabricated separately and then the pressure vessel was tested under fatigue loading.

[1,2 & 3] Department of Mechanical Engineering, UET Taxila, Pakistan

Fatigue Test Description

The pressure vessel was subjected to an internal pressure fluctuation between 0 and 52.5 bars using water as hydraulic fluid. Each cycle has time duration of about 20 Seconds. For stress measurement, five bi-axial strain gauges were applied on different positions. In addition two acoustic sensors were also used for online monitoring of acoustic emissions during pressure fatigue test. The stresses observed were well below the material yield limit. High amplitude acoustic emissions were observed at about 5000 cycles. The amplitude of signals was raised in later cycles as shown in Figure 1. The high emissions indicate the crack initiation and growth. The test was continued for further cycles until we got highest amplitude about 100 dB.

Table 1: Designed Pressure Vessel Dimensions

Part of Vessel	Parameter	Calculated Value	Used Value
Shell	Thickness	3 mm	3 mm
Flat Head	Thickness	17.5 mm	17.5 mm
	Radius of inner corner	9.5 mm	9.5 mm
Nozzle	Thickness of cylinder	0.67 mm	3 mm
	Radius of inner corner	1 mm	1 mm
	Thickness of flange	638mm	65mm

Fatigue Evaluation by ANSYS

ANSYS was used as the primary tool for obtaining cyclic elastic-plastic finite element solution of the current problem. The numerical stress analysis of the critical details identified in previous section was carried out using nonlinear finite element method. The S-N curve for the material "SA 516-G70" is corrected by data available in ASME code. The loading type considered is constant amplitude zero based. The appropriate stress concentration factors are also provided for correcting alternating stresses at such critical areas. Moreover the strain hardening parameters are also given to the software for evaluating plastic strains. The pressure vessels modeled and tested under the same condition as it was tested in actual. The pressure vessel was failed from inner corner of nozzle after 5051 cycles. This result is very close to the fatigue life analyzed by ANSYS.
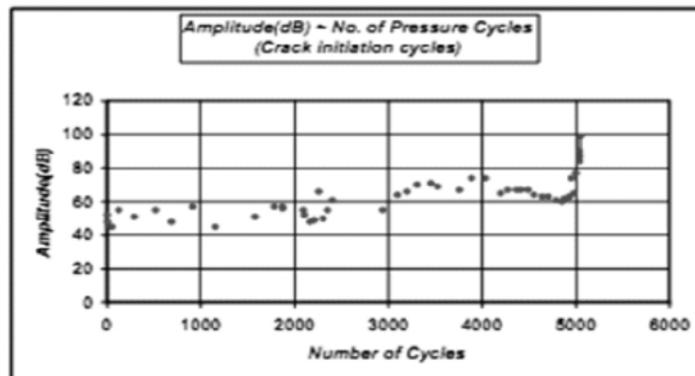
Figure 1: Number of cycles Vs Amplitude

Comparison of Results

The vessel used in this research work was designed for a life of 4500 cycles. The fatigue life analyzed by ANSYS is 5234 whereas experimental results showed an actual life of 5051 pressure cycles. The FEA and experimental results are very close to each other as shown in Figure 2. Experimental stress analysis results are also similar to the FEA results. The stresses evaluated by both techniques are very close to each other in all three main regions of pressure vessel as shown in Figure.3. Cyclic elastic-plastic FEA results showed that the nozzle inner corner is the weakest area from fatigue point of view. These FEA results are also validated experimentally because vessel was failed from same inner corner of nozzle.

Conclusions

ASME-BPV code, although conservative, cannot evaluate the exact fatigue life of a pressure vessel because; it provides the fatigue evaluation procedure for individual parts of a pressure vessel and not for an assembled pressure vessel. Whereas the cyclic elastic-plastic FEA proved very useful to predict the overall fatigue life of such pressure vessels. The slight difference in experimental and numerical results occurred because of some manufacturing laps, software limitations and short duration of pressure cycles. Shift in the experimental and numerical results is there but the overall behavior seems to be identical. The elastic-plastic state of stress is observed at nozzle inner corner in this case. It proves that although well designed pressure vessel could have some localized areas where yielding may occur. It is recommended for design engineers to evaluate such areas by FEA to save time and fabrication cost. Acoustic emission monitoring during hydrostatic and cyclic pressure testing proved very useful to judge the crack initiation and crack propagation phases of tested pressure vessel. Through FEA, we can minimize the total design and analysis time. Moreover complex and stress concentrated areas of pressure vessel can be evaluated quickly and accurately.
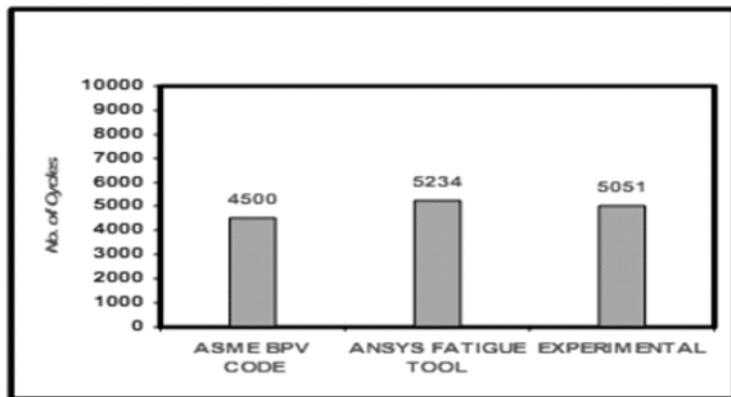
Figure 2: Fatigue life of Pressure Vessel
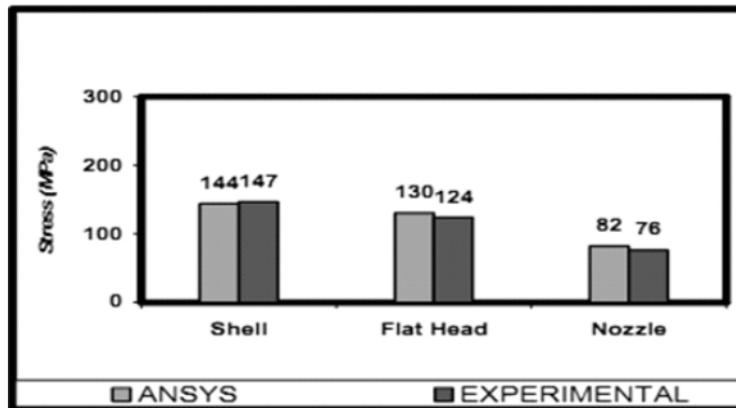
Figure 3: Stresses in Pressure Vesse

References

[1]   Ed. Nigel Taylor, "Current practices for design against fatigue in pressure equipment", EPERC bulletin 6, June 2002.

[2]   Changes S.C. Chu,, "Elastic- Plastic deformation of cylindrical pressure vessels under c y c l i c loading, International journal of pressure vessels and piping, Volume 31, issue 2 Page 228-237 May 1974.

[3]   ASME Boiler and Pressure Vessel Code, Section VIII, Division 2," Rule for Construction of Pressure Vessels-Alternative Rules", The American Society of Mechanical Engineers, New York, 2001 Edition and 2002 Addenda.

Effect of Geometric Imperfection on Buckling Strength of Cylindrical Shells

Khurram Shahzad[1], Sagheer Ahmed[2] and Himayat Ullah[3]

Abstract

In this research paper, effect of geometric imperfection on buckling of cylindrical shell subjected to different types of loadings has been investigated using Finite element analysis and compared with analytical model by Donnell and semi Empirical model based on experimentation [1,2] of a perfect shell. In finite element analysis Newton Raphson and Arc length methods are used. Based on the presented results conclusions can be drawn concerning the shell behavior and its sensitivity to different loadings.

Keywords: FE Analysis, Buckling Strength, Geometric Imperfections, Bifurcation.

Introduction

The shell structure is typically found in nature as well as in classical architecture [3]. Cylindrical shells have been extensively used in all types of structures. They are subjected to various loading both static and dynamic in nature. Among the most common types of loading are the axial compression, bending, torsion and lateral pressure, which not only challenge the strength of the structure but could also cause deformation of unacceptably large amplitude and could lead to loss of stability and collapse of the whole structure.

Distributed loads due to internal pressure in storage tanks, pressure vessels or silos or to external pressure from wind, marine currents and hydrostatic pressures are very well resisted by the in-plane behavior of shells. On the other hand, concentrated loads introduce significant local bending stresses which have to be carefully considered in design. Such loads can be due to vessel supports or in some cases, due to abnormal impact loads in containment buildings of nuclear power plants, for example, codes of practice usually require the possibility of missile impact or even sometimes airplane crashes to be considered in the design. In these cases, the dynamic nature of the load increases the danger of concentrated effects.

The theoretical limits of bifurcation of equilibrium that can be reached using mathematical Models are upper limits to the behavior of actual structures; as soon as any initial displacement or shape imperfection is present, the curve is smoothed [4]. It is well known that the linear buckling prediction of thin shell is purely theoretical and it should be reduced in order to account for the influence of geometric imperfection and other defects.

The difference in behavior, compared with that of plates or bars, can be explained by examining the pattern of local buckling as the loading increases. Initially, buckling starts at local imperfections with the formation of outer and inner waves the latter represent a flattening rather than a change in direction of the original curvature and set up compressive membrane forces which, along with the tensile membrane forces set up by the outer waves, tend to resist the buckling effect. At the more advanced stages, as these outer waves increase in size, the curvature in these regions changes direction and becomes inward as a result, the compressive forces now precipitate buckling rather than resist it, thus explaining why equilibrium, at this stage, can only be maintained by reducing the axial load.

Geometric imperfections caused by manufacturing are the main cause of the significant differences between critical buckling loads calculated using classical methods and experimental buckling loads. Even very small imperfections can cause a substantial drop in the buckling load of the shell. The sensitivity to imperfection depends primarily on the type of shell and type of loading, and, to some extent, on the boundary conditions. It may vary from moderate to extreme, even for the same shell geometry under different loading or boundary conditions. For example, a cylinder under axial Compression is extremely sensitive to imperfections whilst the same shell under external pressure exhibits much lower imperfection sensitivity.

[1,3] NESCOM, Islamabad, [2] MED UET Taxila

Bifurcation Buckling [5]

If a structure is subjected to a given load and large increase in load results in a large change in the equilibrium configuration of shell, the applied load is defined as buckling load and the emerging geometry is called the buckling mode. The change in equilibrium configuration is usually a large increase in the deflection of shell, which may or may not be accompanied by change in the basic shape of shell. There are two types of buckling; bifurcation and nonbifurcation. A bifurcation point is a point in load history where two branches of the solution are possible. The most common example of bifurcation buckling is the buckling of simple column. The general shape of the load-deflection curve for such a member is shown in Fig 1. Cylindrical shells are more subjected to bifurcation buckling.

Proposed Methodology for Nonlinear Buckling Analysis

The methodology is based on the following steps:

Linear buckling analysis

- FE analysis for cylindrical shells
- Analytical solution for shells under axial compression, bending, torsion and radial pressure.
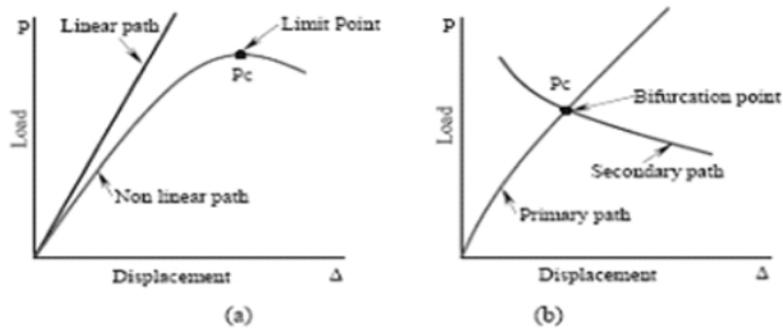

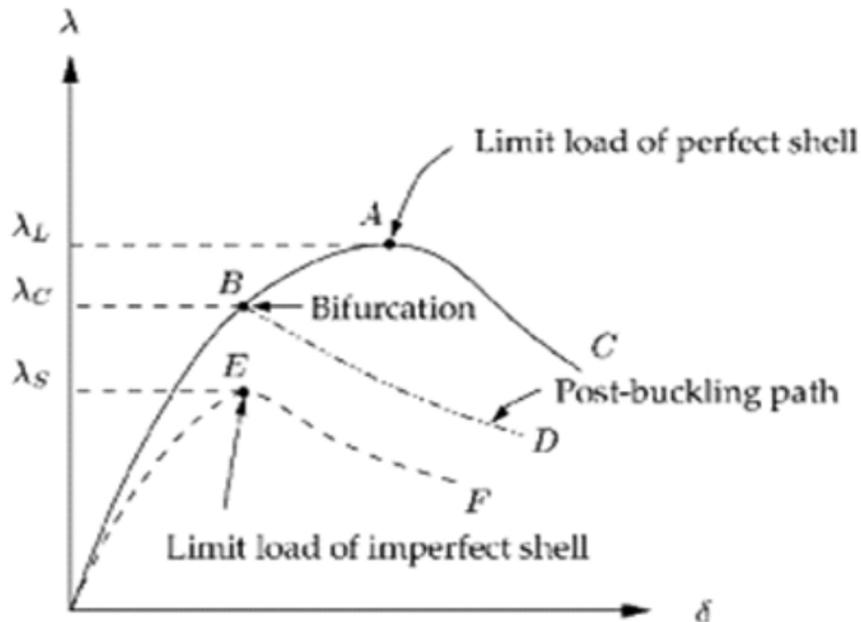Figure 1: Load-deflection curve showing bifurcation point and limit point

Figure 2: Effect of imperfection on limit load

Nonlinear buckling analysis

- FE nonlinear analysis of shell
- Semi empirical model by introduction correction factors in analytical model

The methodology is explained in the next section and all the above points are applied to specific shell.

Geometry & Material Characteristics of Cylindrical Shell

An aerospace structure has a circular cylinder of diameter 1500 mm, Length 1000 mm and thickness 2 mm. This cylinder is subjected to various types of loads such as axial compression, bending, torsion and external radial pressure. The cylinder is made of Aluminum Alloy Al 2219- T6 having Young's modulus of 71.7GPa. We have to calculate the buckling strength under these loadings.

Geometric Nonlinearity

Geometric nonlinearity [7] is added in the model by reducing the thickness of the cylinder by factor of 10% along the length of cylinder. $\delta/t = 0.1$.

Table 1: Physical Properties of Model

Cylinder Height	1000mm
Cylinder Diameter	1500mm
Cylinder Thickness	2 mm
Material	Aluminum 2219-T6
Young's Modulus	71.7 GPa
Poisson's ratio	0.33
Yield Strength (1.2-6mm plate)	248 MPa
Tangent Modulus	1824 MPa

Linear Buckling Analysis of Cylindrical Shell

FE (Eigenvalue) Analysis of Shell

Eigenvalue buckling analysis predicts the theoretical buckling strength of an ideal linear elastic structure. A 3-D model was built for a cylindrical shell of the dimensions given in the table, using ANSYS 9.0 finite-elements software. The cylinder under discussion is modeled with Shell 181 element having six degrees of freedom, 3 translations in X, Y and Z direction and 3 Rotations about the same axes. The shell was meshed using quadrilateral shaped elements. The mesh size used is 15 mm on both circumferential and longitudinal (axial) sides. This degree of mesh size refinement was chosen based on convergence calculations carried out. This meshing scheme results in approximately 21,172 elements and 35,000 active degrees of freedom.

Analytical Solution of Shell [8,9,10,11]

Axial Compression Strength, Pth = 0.10928*107N

Bending Strength, Mth = 506.8KN-m

Torsional Strength, Tth = 157.2KN-m

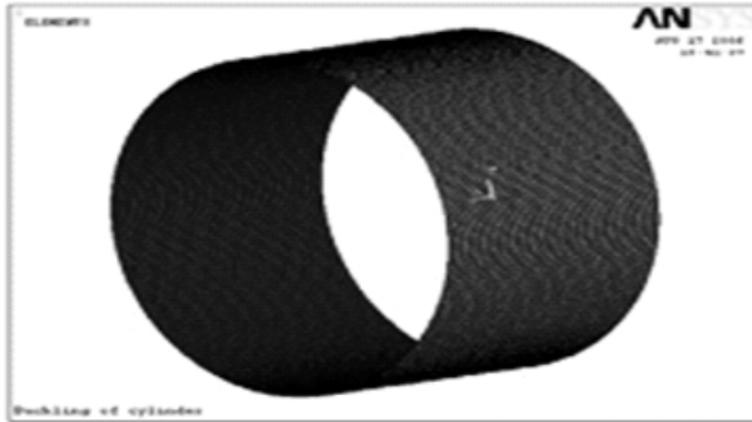External Radial Pressure Strength, Pth = 0.02117 MPa
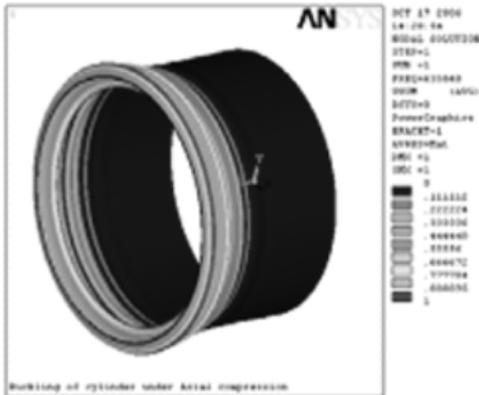

Figure 3: Finite Element Model of Cylinder

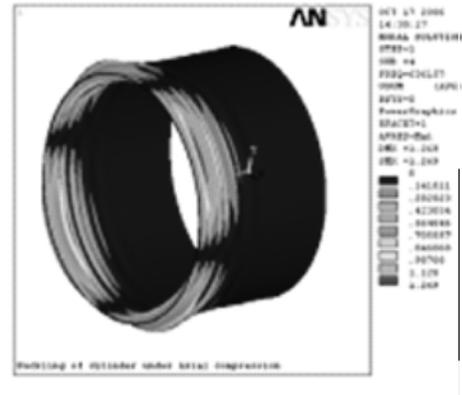Figure 4: 1st mode shape (Axial compression)

Figure 5: 4th mode shapes (Axial compression)
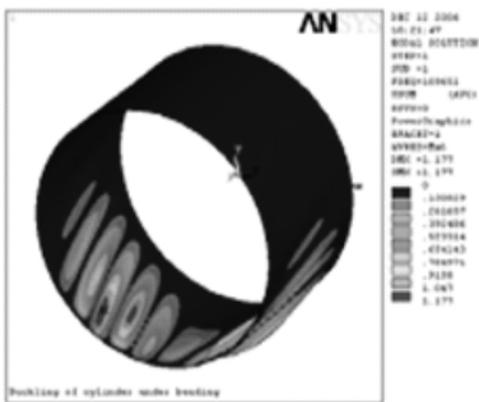

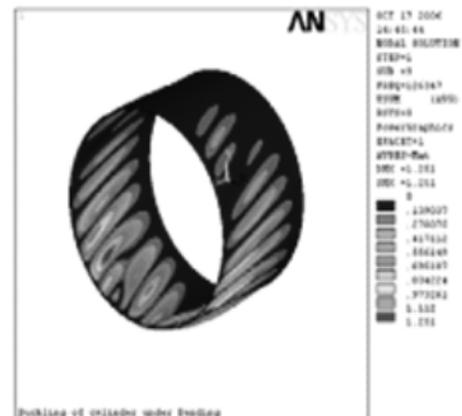Figure 6:1st mode shape (Bending)

Figure 7: 9th mode shape (Bending)

Nonlinear Buckling Analysis of Cylindrical Shell

A nonlinear buckling [12] analysis employs a nonlinear static analysis with gradually increasing loads to seek the load level at which a structure becomes unstable. Using a nonlinear buckling analysis, you can include features such as initial imperfections, plastic behavior [13], contact, large-deformation response, and other nonlinear behavior. In a nonlinear buckling analysis, the goal is to find the first limit point (the largest value of the load before the solution becomes unstable). The arc-length method [14] can be used to follow the post-buckling behavior. Nonlinear buckling is more accurate than eigenvalue buckling, and is therefore recommended for the design or evaluation of structures.
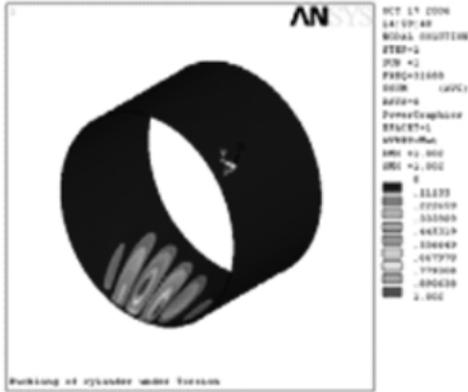
Figure 8: 1st mode shape (Torsion)

Figure 9: 8th mode shape (Torsion)

Figure 10: 1st mode shape (Pressure)
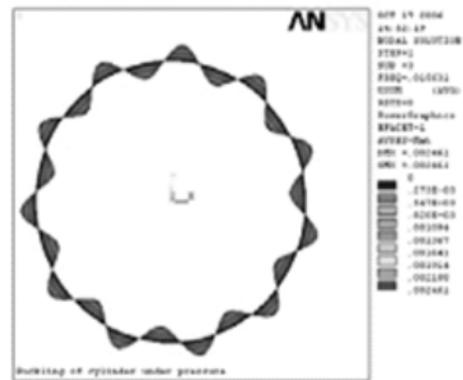
Figure 11: 3rd mode shape (Pressure)

Semiempirical Solution of Shell Buckling [8,9,10,10,13]

Axial Compression Strength, $P_{th} = 0.10928 \times 10^7 N$

Applying plasticity correction factor, $P = 0.162141 \times 10^6 N$

Bending Strength, $M_{exp} = 155.4 KN\text{-}m$

Applying plasticity correction factor, $M = 24.696 KN\text{-}m$

Torsional Strength, $T_{exp} = 121.6 KN\text{-}m$

Applying plasticity correction factor, $T = 77.574 KN\text{-}m$

External Radial Pressure Strength, $P_{exp} = 0.02117 MPa$

Applying plasticity Correction factor, $P = 0.003413 MPa$
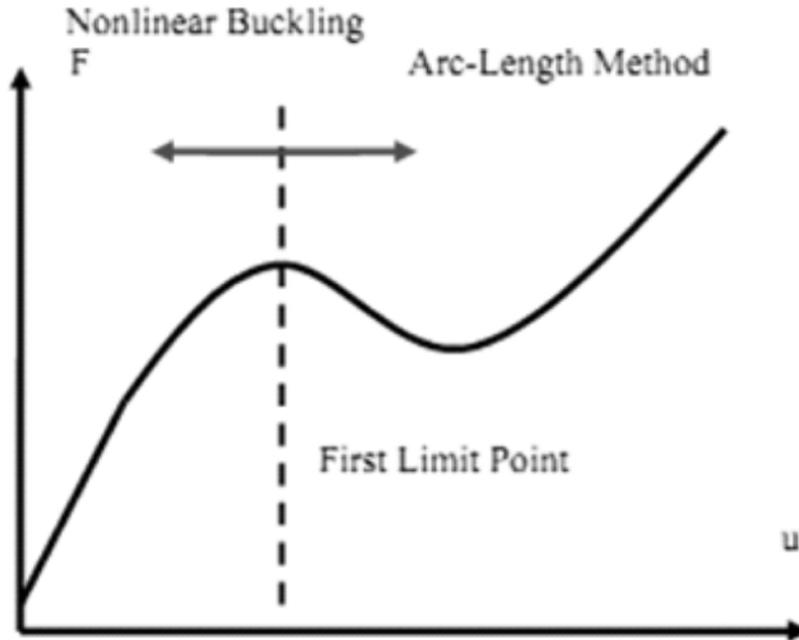
Figure 12: Nonlinear Buckling
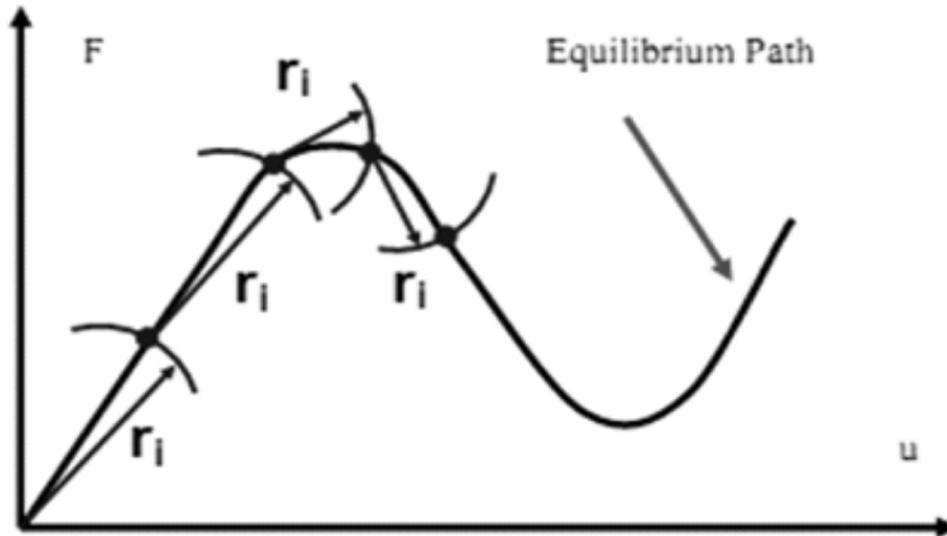
Figure 13: Arc Length Method

Load vs Displacement Graph for Nonlinear Buckling in FEA

Discussion of Results

Application of theory to the design of actual cylindrical shells is complicated by apparent discrepancies between theory and experiment [13]. The table given below compares the Buckling loads of case study cylinder subjected to axial compression, bending, torsion and external radial pressure using theoretical, experimental and FEM approach. The FEM results are based on lowest factor obtained from eigenvalue buckling analysis for linear analysis and for nonlinear analysis the limit load value.
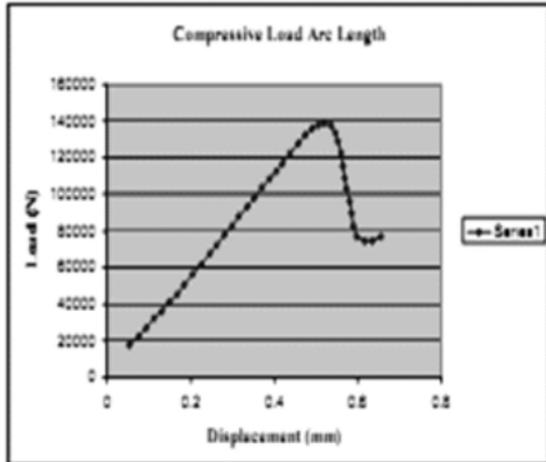
Figure 14: Arc Length method graph (Axial compression)
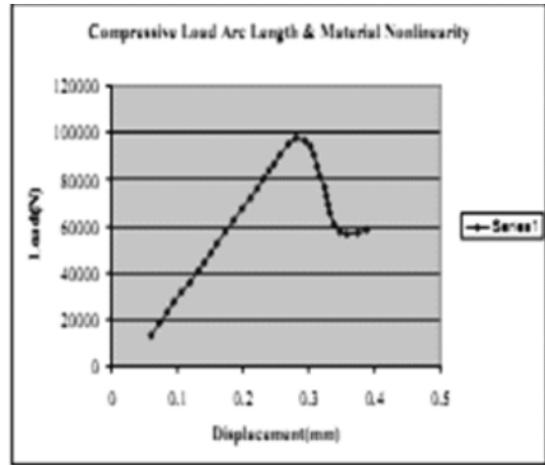
Figure 15: Arc Length method graph with material nonlinearity (Axiacompression)
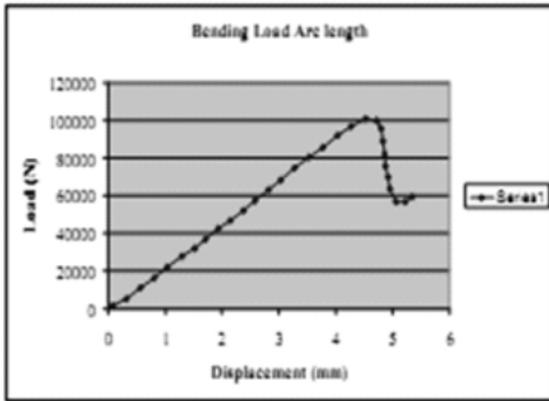
Figure 16: Arc Length method graph (Bending)
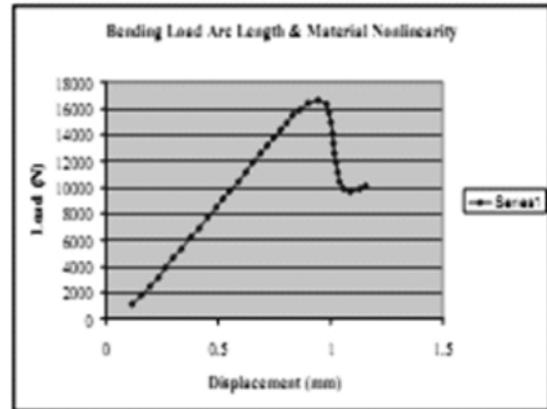
Figure 17: Arc Length method graph with material nonlinearity (Bending)
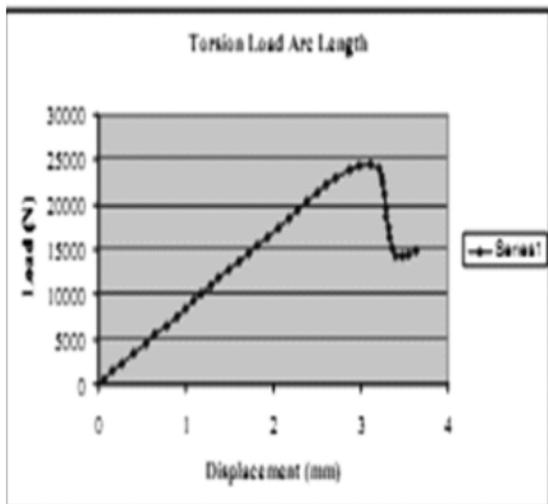
Figure 18: Arc Length method graph (Torsion)
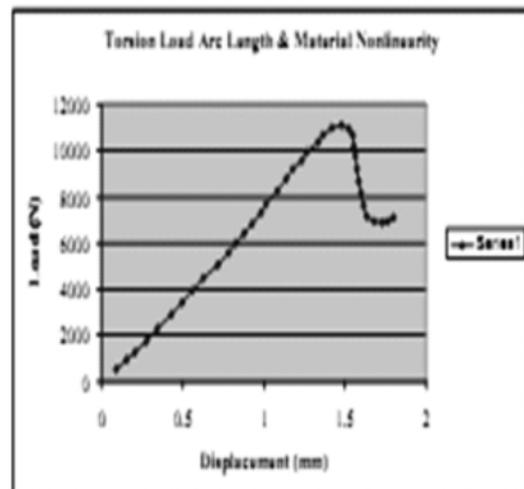
Figure 19: Arc Length method graph with
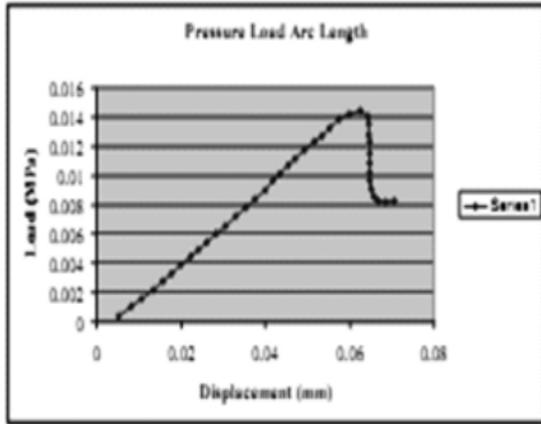
Figure 20: Arc Length method graph (Pressure)
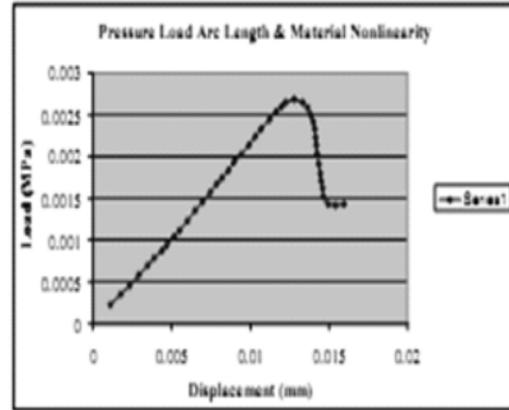
Figure 21 Arc Length method graph with material Nonlinearity (Pressure)

Table 2: Comparison of Buckling loads of case study using Theoretical, FEM and Semi-empirical approach in linear & nonlinear behavior

Loading	Linear		Nonlinear	
	Theoretical	FEM	Experimental	FEM
Compressive	0.10928×10^7N	0.11030×10^7N	0.235619×10^6N	0.241×10^6N
Bending	506.8KN-m	168KN-m	155.4KN-m	157.260KN-m
Torsion	157.2KN-m	77.574KN-m	121.6KN-m	60.01KN-m
Pressure	0.02117MPa	0.02322MPa	0.02117MPa	0.0221MPa

Table 3: Comparison of Buckling loads of case study using Theoretical, FEM and Semiempirical approach in material nonlinear behavior for imperfect cylinder

| Loading	Geometric Imperfection		
	Linear	Non linear	Material Nonlinearity
Compressive	0.63585×10^6N	0.138923×10^6N	0.097895×10^6N
Bending	109.65KN-m	102.643KN-m	16.634KN-m
Torsion	47.532KN-m	36.7703KN-m	16.6647KN-m
Pressure	0.015172MPa	0.014403MPa	0.0026858MPa

Conclusions

1. There is large discrepancy between theory and design data for buckling loads. For shells in which longitudinal compression of the cylinder wall is included such as compression the discrepancies can be small between FEM results and experimental results but for bending the variation between two results is large theoretical buckling value is 3.01 times more than numerical value. For shells in which shear of circumferential compression predominates such as external pressure and torsion, the discrepancies are generally less severe. But in case of torsion theoretical buckling load value is 2.02 times more than numerical value.

2. Buckling load is reduced due to material nonlinearities & geometric imperfection.

3. Result shows that in axial compression buckling strength reduces by 1.71 times, in bending buckling strength reduces by 4.62 times, in torsion loading case buckling strength reduces by 3.3 time and in external pressure case buckling strength reduces by 1.4 time.

4. These results show that geometric imperfection has major effect on buckling strength and behavior of shells under different loading conditions.

5. From results it is shown that shells is more sensitive to buckling in bending load as there is large difference between theoretical and numerical results so we can't predict the exactly buckling load.

6. But for buckling load ,the most severe load case study is external pressure as it resulted in lowest buckling strength.

References

[1]   Donnel L.H, "Stability of Thin Walled Tubes under Torsion" NACA Report 1979.

[2]   Batdorf ., S.B. "A simplified Method of Elastic Stability Analysis for Thin Cylindrical Shells". NACA Report 874. 1947.

[3]   Tossoji, Ei., "Philosophy of Structures", Holden Day 1960.

[4]   Brush, D.O., Almroth, B.O.,"Buckling of Bars, Plates and Shells", McGraw Hill, 1975

[5]   Owen F. Hughes., "Ship Structural Design: A Rationally-Based, Computer-Aided Optimization Approach". 1988

[6]   Prof. Dr. J. Arbocz., "Stability analysis of anisotropic shells of revolution under axisymmetric load with general boundary conditions". Faculty of Aerospace Engineering, Delft University of Technology, 1999-2000

[7]   Rudy Alforque., "Hydrostatic & Gravity Loads". ICC Buckling Study, part III, 1997

[8]   Harris, Seurer, Skeene & Benjamin, "The Stability of Thin Walled Unstiffened Circular

[9]   Cylinders Including Effects of Internal Pressure", Jour. Aero Sciences. Vol 25,August1958

[10]   Batdrof, Schildcrout & Stein, "Critical Stress of Thin Walled Cylinder in Torsion" NACA 1344, 1947.

[11]   Siede & Weingarten,"On the Bending of Circular Cylindrical Shells Under Pure Bending", Journal of Applied Mechanics. Vol. 28, March 1961.

[12]   E. F. Bruhn, B. S., M. S., C. E., Dr. Eng., "Analysis and Design of Flight Vehicle Structures". Professor (Emeritus) of Aeronautics and Astronautics Purdue University.1973.

[13]   Baker E. H., Kovalevsky L. & Rish F. L., "Structural Analysis of Shells", McGraw-Hill Book Company, New York, 1972.

[14]   NASA SP-8007,."Buckling of thin walled circular cylinder" NASA, Space vehicle designcriteria, 1968.

[15]   Simcon International, "Ansys advance training", Karachi Pakistan. 2003.

Configuration Management of EN 30B Steel Parts Machining Processes

Khalid Hussain[1] and Khalid Mahmood[2]

Abstract

The processes involved are supporting documents, designing phase, Computer Numeric Control (CNC) machining, heat treatment, NDT and Quality Assurance for producing final product EN30 B steel parts in a local industry. Every product made will be a part of an assembly and every assembly will be part of the complete assembly. At the end when all assemblies integrate, it is the completion of the project. Each project must have its own identification number in the Configuration Management (CM). Many of these assemblies are also called Configuration Item (CI). This will have a serialized unique number for identification in CM, on the basis of each project. The manufacturer identifies that part from its identification number and implements the processes according to the instruction. The manufacturing processes for making part lies in two categories one is called Critical and the other as Non-Critical.

The CNC machining has two methodologies that is (a) to machine the component using the programming options provided by the manufacturer. (b) The second aspect involves, Computer Aided Manufacturing (CAM), which has very lengthy procedures that makes it impossible to maintain the quality of the product. The programs are executed in two stages Roughing and Finish Machining. The parts are heat treated to desired hardness level of 47-50 HRC after the rough machining and then the parts are finish machined to the required sizes and tolerances. At this stage, component is sent for de-burring and tapping and then it undergoes NDT by using dye penetrent method. The parts are given cadmium plating as a surface treatment and then the final Quality Assurance (QA) inspection.

Keywords: Configuration Management, Configuration Item, Computer Numeric Control, Computer Aided Design, Computer Aided Manufacturing, NDT, Cadmium Plating, EN 30B Steel.

Introduction

The first step to start manufacturing a part requires drawing from the Configuration Management section. The responsibilities of in charge manufacturing section are (a) to Raise a form for issuance of the complete documents for that part, (b) getting the required materials (c) and allocation of the drawings.

The concern section will study the drawings and then complete the job by including necessary tooling, fixtures, gauges, and equipments needed for production of parts.

Selection of the required program for making the component is based on two methodologies (a) manual (b) and Numeric Control (NC) Data. For manual program, the operator will use Computer Aided Design (CAD) and for NC data, by using different software's i.e. Pro-E and Quick CAM etc [1]. After generating code, for verification a simulation run is made by using machine graphics. After setting as per required program for the CNC machine, its feed and speed is calculated, according to the material specification. The four basic ideologies for successful running the Configuration Management System are, (a) all data and equipment items must be identified, (b) and an individual or a group will be responsible for issuance and control of all configuration identifiers. (c) Then a system is established with written procedures for controlling identification operations. (d) An independent control group is established to verify correct identification procedures for the manufacturing processes involved.

Tool Life Management

Tool life management is very important in the manufacturing processes for making a quality product. The life of all those tools which will be involved in the processing of the part must be measured and calculated. This is necessary both for machine and also for tools. The tool coolant is a necessary in machining operation. Process inspection should be carried out at each stage, so that chances of error should be minimized [1].

[1,2] National Engineering and Scientific Commission, Islamabad.

Machining Process

To develop a perfect and accurate metal parts the CNC machine is the best.   Table-1 is the sequence of the machining process (NC Data) to manufacture a part. The NC data is guide line for CNC machine.

Heat Treatment

The EN30B Steel is purchased in annealed condition for ease in machining. After rough machining it is required to be heat treated to achieve the hardness between 47~51 HRC. For this purpose, the parts are heated to 820°C and held at this temperature for half hour [2]. This time is based on the maximum section thickness of the component. As there are some dimensions which are finally machined at this level, for example threads which are tapped, therefore it is recommended to heat treat the components in a vacuum furnace. If not treated in a vacuum furnace, the scale will appear on the parts surface which will result into a lost of tolerances dimensions. Then the parts are quenched oil. At this stage, residual stresses are induced in parts due to thermal gradient in the quenching process. Therefore, after hardening it is recommended to temper at 190-200°C for one hour to achieve the desired hardness range and get rid off residual stress [3].

Surface Treatment

The surface treatment of the metallic parts is usually done to protect the part from environmental attack. Different surface techniques which can be used i.e. (a) Cadmium Plating, (b) Zinc Plating, (c) Electroless Nickel Plating and Phosphateing.

Table 1: Sequence of Machining Processes (Nc Data):

(F25B)	N3.8X558.496	N7.8X558.496	N10.8X-20.
N1.0G71	N3.9Y2.171	N7.9Y6.118	N10.9Y9.066
N1.1G17	N4.0X-20.	N8.0X-20.	N11.0X558.496
N1.2G90	N4.1Y2.368	N8.1Y6.316	N11.1Y9.261
N1.3T0101M13	N4.2X558.496	N8.2X558.496	N11.2X-20.
N1.4S1500M3E01	N4.3Y2.566	N8.3Y6.513	N11.3Y9.457
N1.5G0X-20.Y0.	N4.4X-20.	N8.4X-20.	N11.4X558.496
N1.6Z100.	N4.5Y2.763	N8.5Y6.711	N11.5Y9.653
N1.7G1Z32.618F50	N4.6X558.496	N8.6X558.496	N11.6X-20.
N1.8X558.496	N4.7Y2.961	N8.7Y6.908	N11.7Y9.849
N1.9Y.197	N4.8X-20.	N8.8X-20.	N11.8X558.496
N2.0X-20.	N4.9Y3.158	N8.9Y7.105	N11.9Y10.044
N2.1Y.395	N5.0X558.496	N11.8X558.496	N12.0X-20.
N2.2X558.496	N5.1Y3.355	N9.0X558.496	N12.1Y10.24
N2.3Y.592	N5.2X-20.	N9.1Y7.303	N12.2X558.496
N2.4X-20.	N5.3Y3.553	N9.2X-20.	N12.3Y10.436
N2.5Y.789	N5.4X558.496	N9.3Y7.5	N12.4X-20.
N2.6X558.496	N5.5Y3.75	N9.4X558.496	N12.5Y10.631
N5.5Y3.75	N5.6X-20.	N9.5Y7.696	N12.6X558.496
N2.7Y.987	N5.7Y3.947	N12.4X-20.	N12.7Y10.827
N5.6X-20.	N5.8X558.496	N9.6X-20.	N12.8X-20.
N2.8X-20.	N5.9Y4.145	N9.7Y7.891	N12.9Y11.023
N5.7Y3.947	N6.0X-20.	N9.8X558.496	N13.0X558.496
N2.9Y1.184	N6.1Y4.342	N9.9Y8.087	N13.1Y11.219
N5.8X558.496	N6.2X558.496	N10.0X-20.	N13.2X-20.
N3.0X558.496	N6.3Y4.539	N10.1Y8.283	
N5.9Y4.145	N6.4X-20.	N10.2X558.496	
N3.1Y1.382	N6.5Y4.737	N10.3Y8.479	
N6.0X-20.	N6.6X558.496		
N3.2X-20.	N6.7Y4.934		
N6.1Y4.342	N6.8X-20.		
N3.3Y1.579	N6.9Y5.132		
	N7.0X558.496		
	N7.1Y5.329		

We applied cadmium plating to give excellent rust protection, especially in the marine environment [4]. The plating layer of 8-12 micron is required. After cadmium plating, steel parts are subjected to de-embritlement process, at 190°C for 23 hours in furnace [5]. Usually the steel parts having UTS greater then 1000 MPa are subjected to de-embritlement process and as the UTS increases baking time also increases. The purpose of this process is to remove the nascent hydrogen which is induced in the parts during electroplating process. avoiding the process results into decreasing the mechanical prosperities of the steel parts, especially impact properties.

Configuration Management

The successful methodology for the completion of parts is to identify the complete and accurate information through Configuration Management. To fulfill the customer's requirement for performance of a part in the field is not possible, without ample identification. With an organize mechanism all the components of a system will be tied together into a uniform package before going into the manufacturing processes.

(a) General Requirement

To accomplish the user requirement through identifying and inter relating the parts assemblies in the project the associated documents must be accepted by the user. There are seven key points to achieve the target and to meet the user requirements:

(a) Identification of contract information

(b) Drawings and engineering data

(c) Deliverable parts and data

(d) Technical information

(e) Change information

(f) Acting in accordance with customer acceptance procedures

(g) Acting in accordance with inspection

(h) Demonstration requirements

For different parameter involved in this procedure [6] see Figure1.

According to the customer/user requirement, the configuration management officer must focus the main three areas. (a) Compose and assign all configuration identification numbers. (b) apply these numbers to data an
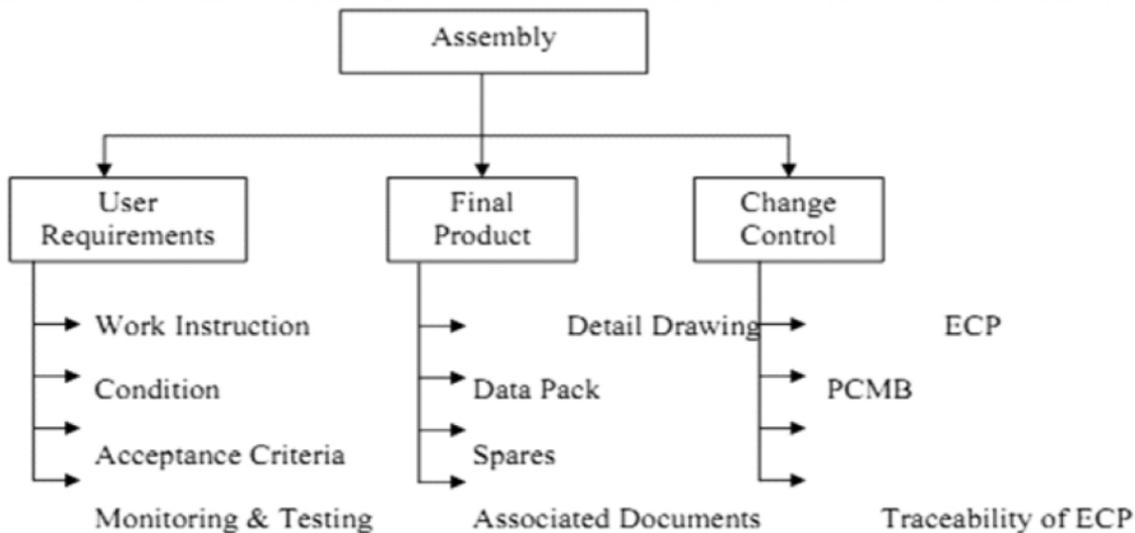

Figure 1: Area of Identification

(b)   User Requirements

There must be an authenticated document in which user's requirements are listed. The Configuration Manager is responsible to generate this document. This document should be approved by the Project Manager, System Engineer, Originator of the document and Configuration Manager. All the terms and conditions must be defined in that document. After signature of all team members this document should archive in document control center with Master Copy stamp. In this document all the necessary information should be mentioned, about the product, the expected results of the product, starting date and final date of the project. There should also be a list of associated documents which will be given to the customer with the product. A formal change criteria, is also the part of this document [6].

(c)   Work Instruction

In this document all the procedures/steps will ensure for an operator or manufacturer.   From a raw material to a finish product, all stages are mentioned according to their sequences over there. If any special instruction is required for manufacturing the part a separate section must be mentioned in this document.

(d)   Acceptance Criteria

After illustration the user requirement, another document which is very important for manufacturer as well as user that is "Acceptance Criteria", in which all parameters will be defined in this document on the basis of which a product / part will be considered as a final product according to the user requirement. When manufacturer design and develop a product according to the requirement and also in the light of acceptance criteria, then final product/part will be acceptable to the user.

(e)   Monitoring and Testing

The QA representative who has been sited in manufacturing premises is responsible for monitor and test the product on each stage. All those steps on the basis of which a user will accept that product has been mentioned in "Acceptance Test Criteria". In the light of Acceptance Criteria all the testing and monitoring will be carried out. On the basis of Acceptance Criteria QA has been generating a document "Inspection Test Instruction". This document is supposed to be a rod map for QA rep for monitoring and testing according to the user requirement.

(f)   Final Product

After applying all processes from work instruction to monitoring and testing, a raw material convert in final product/finish product. The more documents or helping documents will be required for support and archive the history of the product, i.e. (a) Detail Drawing, (b) Data Pack, (c) Spares, (d) and associated documents.

(g)   Detail Drawing

Detail drawing of a part is the basic document for production. It this document is issued from configuration management office, it consider as an authenticated and latest document for production. Each drawing of a part also contains the information about its "Next Higher Assembly" and also "Used On". This information is placed on the top right corner of the drawing. The issue no. of a drawing is the important information about the latest version of the part. When an issue is changed, the Engineering Change Procedure will be carried out for updating the drawings.

Engineering drawing and data

In this document all dimensions, tolerances etc will be mentioned. This document has also contained the nomenclature of the part, unique number with reference to assembly and information about the next higher assembly (main assembly) and used on (CI) information. Detail drawing, parts list, "Family Tree" is required to identify the design and elaborate the breakdown of each step in the system. With the help of the

family tree a system or project can be identified easily that is from main system to the last part of the project is identified. The family tree is the key document to explain the system's assemblies, sub-assemblies, sub-sub-assemblies of making a part. All associated documents are also reflected in this document as shown in Figure -2 [6].

(a) Engineers Support

Practitioners rejected the early systems because they were helping the configuration manager, and bothering everybody else major move toward acceptance was to consider the software programmer as a major target customer: helping him/her in the usual Software Engineering (SE) activity became basic service [6].

Conclusion

The Configuration Management for both Hardware and Software is a mechanism to identify for all data, equipment items and configuration identifiers. This identification must provide facility to uniquely identify and select any metal part or its documents. The identification must be consistent and have uniform format. The tools life of all those processes which are involved in the machining of the parts must be measured and calculated. Cadmium is used to give excellent rust protection especially in marine environment. The plating layer thickness was 8-12 micron. The specifications, requirement and procedure of all the machining processes must be identified through associated documents to have a control over these processes. The successful methodology for the completion of parts is to identify the complete and accurate information through Configuration Management.

Acknowledgement

We are thankful to our organization which provided us invaluable help in the completion of this paper.
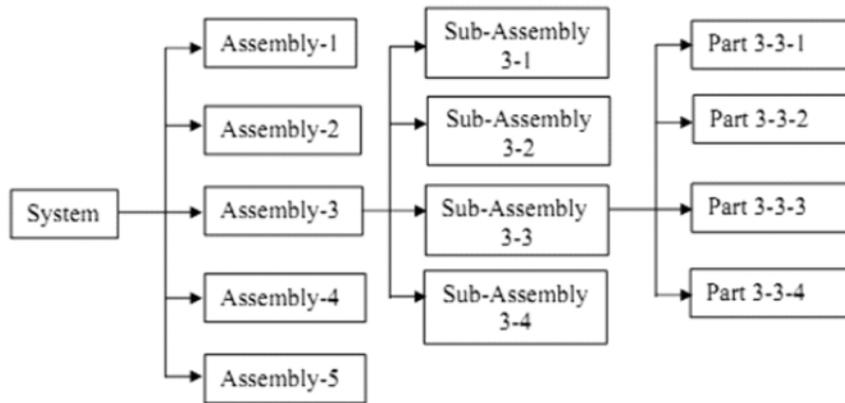
Figure 2: System as per Configuration Management Family Tree

References

[1]   Machining Data Handbook 3rd Edition, Metcut Research Associate Inc Cincinnati.

[2]   William W. Scott Jr. ASM Handbook Ver4.0 Edited by Director of Technical Publication Website   on industrial Heating : www.industrialheating.com.

[3]   Thomas T Samaras "Configuration Management" Deskbook", ISBN 0-934321-   094, Advanced Engineering Consultants Inc.,1988.

[4]   Jacky Estublier. "Software Configuration Management: A road Map" Dassault Systèmes

        LSR, Grenoble University Bat C, Grenoble, France.

[5]   Reidar Conradi, Bernhard Westfechtel "SCM: Status and Future Challenges" Norwegian University of Science and Technology (NTNU) N-7034 Trondheim, Norway.

Usage of Crack Growth Prediction Software Codes for Life Assessment of Aerospace Structures

Waqas Anwar [1] and Nazeer Ahmad Anjum [2]

Abstract

Damage Tolerant Design plays a major role in the Aerospace Industry not only in the design of new structures and components but also their ongoing maintenance and support. Damage Tolerance Analysis (DTA) is a procedure that defines whether a crack can be sustained safely during the projected service life of the structure. Using this methodology, service life of an aerospace structure can be determined and may be extended up to a certain limit as well. Whole procedure for life Assessment of an aerospace structure is very complicated and involves vast area of expertise in Fracture Mechanics, However there is a domain of using state of the art software codes for Crack growth Prediction, Finite Element Analysis and Vortex Lattice Methods.

In this research paper the practical procedure for usage of Crack Growth Prediction Software codes is discussed in details, which is one of the main parts for DTA of any cracked component of an aerospace structure. The same application may be used for life prediction of any other engineering component under fatigue loadings. Mainly the usage of AFGROW code is discussed which is developed by United State Air Force, and available freely for public. For the context and continuity of work other software codes such as PATRAN/NASTRAN for Finite Element Analysis and Athena Vortex Lattice for aerodynamic loads distribution is also discussed secondarily.

Effect of crack growth increment on the convergence of the residual strength is investigated for a wing component of an aircraft. Simulations are based upon Linear Elastic Fracture Mechanics (LEFM) laws that are performed to result the damage scenarios to be assessed in the real structural geometry and loading environment using Stress Intensity Factors, Critical Crack Size, Multiple Sizes Damage and Residual strength calculations. The purpose of this paper is not the publicity of any software company but only to share the experience.

Keywords: Athena Vortex Lattice, AFGROW Code, PATRAN/NASTRAN, FE Analysis, Cyclic Fatigue, Stress Spectrum.

Introduction

1954: 'Metal fatigue' caused Comet crashes (BBC News)

The public inquiry into the Comet airliner disasters has heard that metal fatigue was the most likely cause of two recent crashes. The first crash happened in January, when 29 passengers and a crew of six lost their lives off the Italian island of Elba. The Comet's certificate of airworthiness was withdrawn after second crash, just three months later. Fourteen passengers and seven crew died when the plane went down off the coast near Naples. [1] Cyclic Fatigue is the failure mode associated with repeated loading and is one of the main factors that limit the life of mechanical devices [2]. Damage Tolerance Analysis is necessary to illustrate the process of estimating crack growth behavior, which is used for setting inspection intervals of an air craft. The air craft is then inspected on that declared intervals of time to avoid any catastrophic failure. In this work a major structural member of an aircraft, 'Main Spar Joint to Main Frame' is considered. The analysis goal is to estimate the crack growth behavior of the main spar hole which is more likely under fatigue loadings then other locations.

The requirements before going to Damage Tolerance Analysis involve a number of tasks such as, Usage Spectrum Monitoring, Material Testing of Critical Components and Ground Stress Strain Tests. For more reliability of results Ground Fatigue Teats may be conducted. Output from these tests turns out to be the input of DTA. In case of aerospace structures the provision of Original Equipment Manufacturer (OEM) data may facilitate a lot to reduce number of experiments required for validation of different material properties that plays an important role in crack propagation.

[1] National Engineering and Scientific Commission of Pakistan and [2] MED University of Engineering & Technology, Taxila.
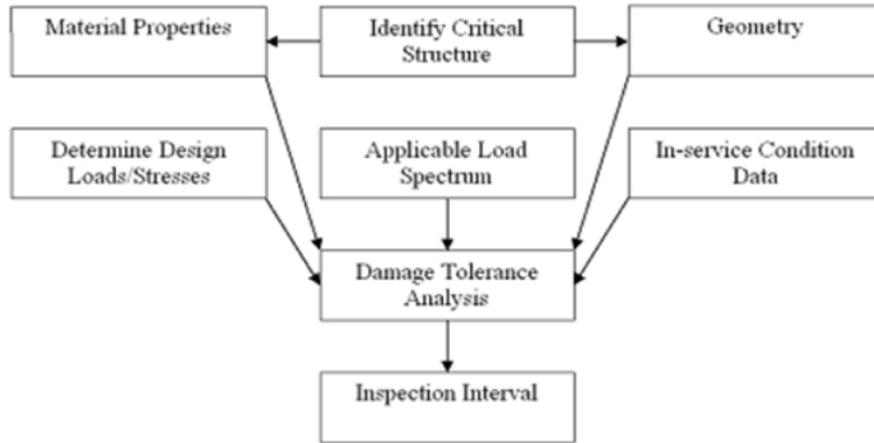
Figure 1 & 2: Flow chart for identifying critical structure & other activities

Identification of Critical Areas

A finite element model was developed using MSC PATRAN 2005r2 which is a three dimensional representation of a functional wing structure. Represented in the model are all spars, ribs, skin and additional secondary structure deemed relevant to the stiffness and load path behavior. After calibration of this model to experimental Ground testing results, the correlated model was run with the aerodynamic loads obtained from Vortex Lattice Method analysis to deliver internal loads input to the Damage Tolerance Analysis.

Figure 3: Internal Load Model of aircraft wing

Figure 4: Critical Area Detection

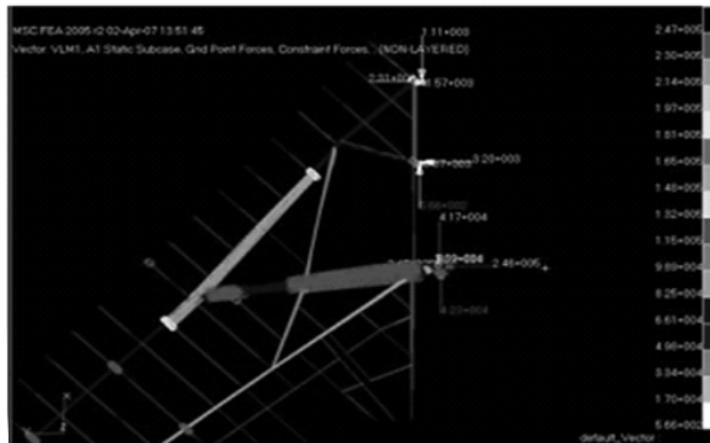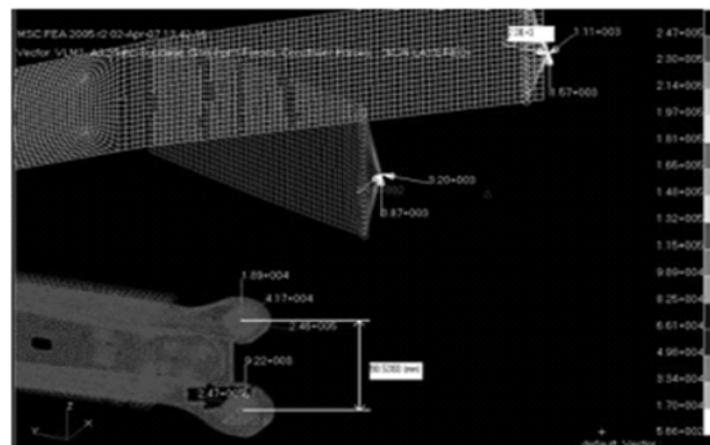It was primarily intended to model the relative load distribution within the wing structure with the focus on main spar to main frame joint. It was expected that any absolute values extracted are to be scaled against known valued or substantiated using an independent analytical approach.

Panel Loads Calculation

Athena Vortex Lattice (AVL) is best suited for aerodynamic configurations. AVL is developed by Massachusetts Institute of Technology and freely available to general public with its user manual. [3].

The wing modeled is mainly consists of thin lifting surfaces at small angles of attack. These surfaces and their trailing wakes are represented as single-layer vortex sheets whose trailing legs are assumed to be parallel to the x-axis. If a fuselage is expected to have little influence on the aerodynamic loads, it is simplest to just leave it out of the AVL model. AVL assumes almost steady flow, meaning that unsteady vorticity shedding is neglected.   More precisely, it assumes the limit of small reduced frequency, which means that any oscillatory motion (e.g. in pitch) must be slow enough so that the period of oscillation is much longer than the time it takes the flow to traverse an airfoil chord.
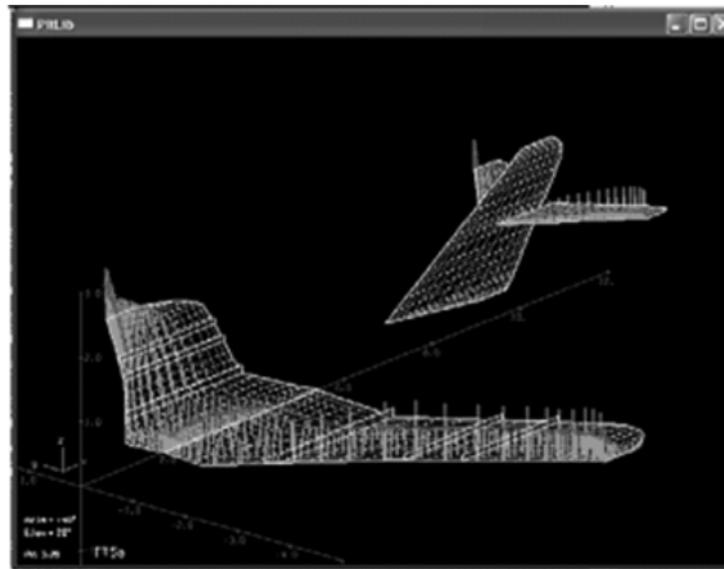
Figure 5: AVL Model Showing Lift Distribution

AVL works with three input files; all in plain text format. Ideally these all have a common arbitrary prefix "xxx", and the following extensions:

xxx.avl   required main input file defining the configuration geometry

xxx.mass   optional file giving masses and inertias, and dimensional units

xxx.run   optional file defining the parameter for some number of run cases

The user provides files xxx.avl and xxx.mass, which are typically created using any text editor. Sample files are provided for use as templates. The xxx.run file is written by AVL itself with a user command. It can be manually edited, although this is not really necessary since it is more convenient to edit the contents then write out the file again.

After getting lift distribution from AVL, the FEA model can be run for these loads, resulting high stress concentration areas. Hence, the component was selected for further DTA after verification of its criticality in air craft structure.

Fatigue Crack Growth Curves

The driving force for fatigue crack growth is described by the range in stress intensity factor

$$(\Delta K = Kmax - Kmin)$$

And fatigue crack growth data are commonly represented on a log-log plot of crack growth rate (da/dN) versus ΔK as shown in Figure6. Typically, three different regions of the FCG curve are considered in developing analytical models to represent empirical data as shown in Figure.6. by the roman numerals. Region I is the "near-threshold" region in which very slow crack growth occurs and where no growth occurs below a threshold value of driving force, denoted as ΔKth. Region II is the linear, steady-state region of the crack growth curve. In the higher growth rate portion of the curve, Region III, rapid and unstable crack growth occurs as final fracture is approached when Kmax equals Kc, the fracture toughness of the material. [4].

Over the years, a number of relationships have been developed to represent all or parts of the typical range of Fatigue Crack Growth (FCG) data, the simplest being the Paris equation [5]. Developed in 1963 to represent the linear region of the curve:

$$\frac{da}{dN} = c \, (\Delta K)^n$$

Where C and n are empirical parameters determined from a curve fit to test data. This original model is still in use today for many applications; more advanced models essentially build on the Paris equation by addressing mean stress effects, threshold behavior (Region I), the instability asymptote (Region III), and fatigue crack closure.
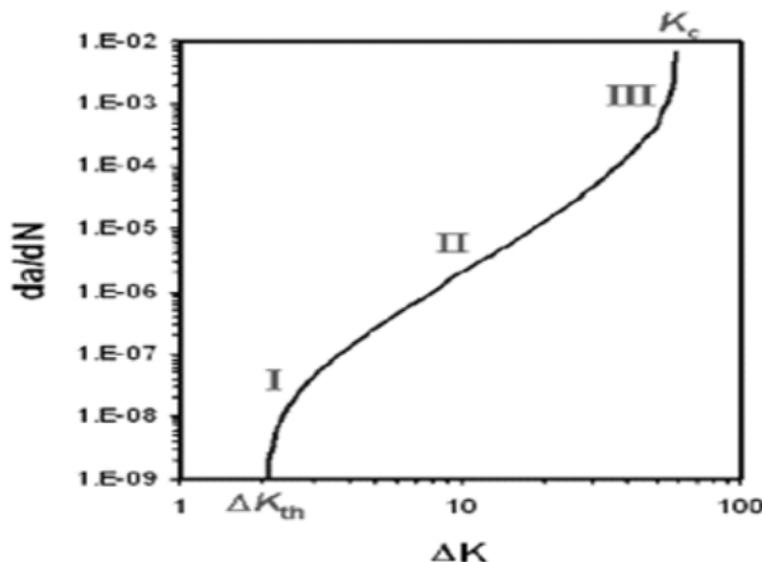
Figure 6: Typical Fatigue Crack Growth Curve Showing Three Regions (I = threshold, II = linear, III = instability)

The Walker equation [6] is a linear model that incorporates mean stress effects through the use of a load ratio, R, where R = δ min/δ max or Kmin/Kmax. The Walker and AFGROW fits are shown plotted against the experimental data in Figure.7. For clarity, the Paris equation has not been plotted. It can be seen from Figure.7 that the NASGRO equation provides a good representation of the knees in the data near the th

reshold region. For the NASGRO equation fits there is some uncertainty as to the fit for the instability region; some conservative judgment was needed in the fitting process in this case. NASGROW database for the selection of material corresponding to crack growth rate curve, is available in AFGROW [7].

Figure 7: Comparison of Walker and NASGROW Curves with the Samples Tested

Material Selection in AFGROW

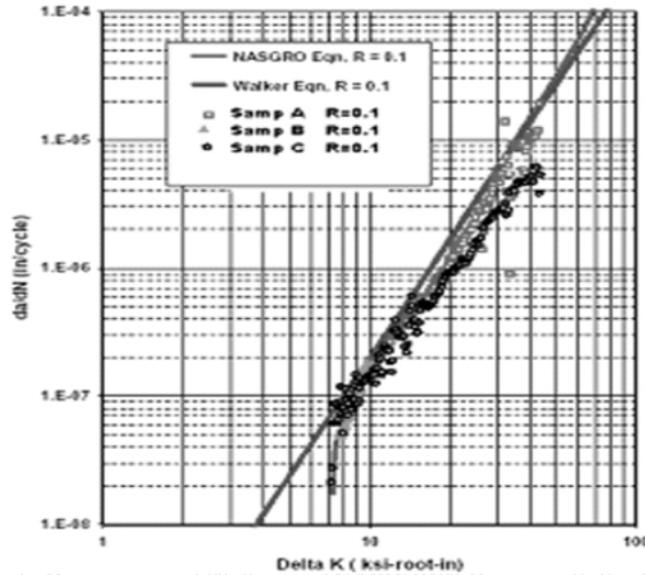Certain parameters were set when a material was selected from the NASGRO material database; AFGROW requires a few parameters that are not directly required for the NASGRO equation. It also allows you to open a previously saved file for a material which may not be available in the database. AFGROW will also allow users to enter data for a single R-value. In this case, the user defined data will be used regardless of the stress ratio for a given analysis. This may be useful in cases where rate data is scarce and the user is only interested in predicting constant amplitude loading (constant R). [8].

Application of Stress Spectrum

AFGROW includes Fighter Aircraft Loading Standard for Fatigue Evaluation (FALSTAFF) spectrum that was applied to selected component geometry. In addition to this user can also define constant amplitude loading spectrum or variable amplitude loading spectrum, according to the application. The Standard FALSTAFF spectrum is show in figure.9.[9]
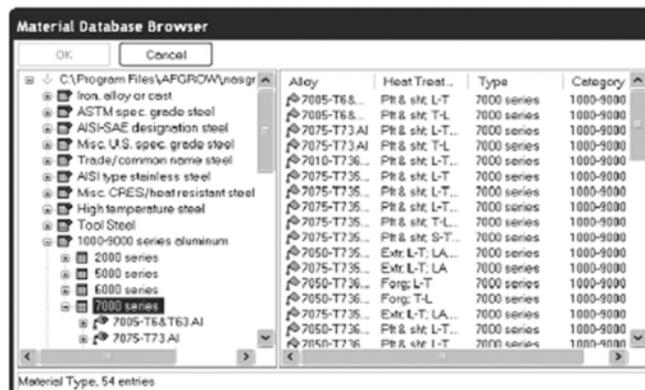

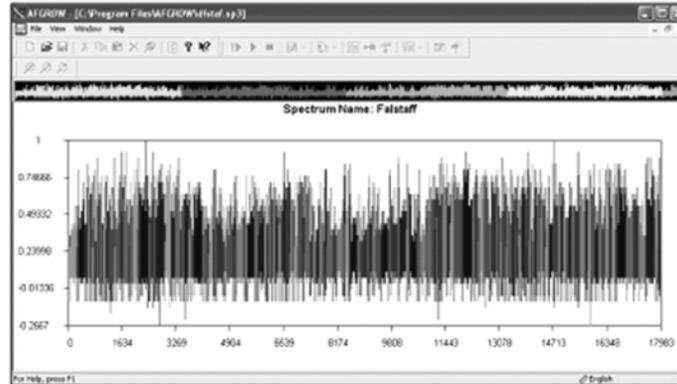Figure 8: material Database browsers in AFGROW

Figure 9: FALSTAFF Loading Spectrums

Results

After providing of all the inputs required in AFGROW, the solution was run, resulting the curve between crack size and number of stress cycles or flight hours, as shown in figure 10. It predicts the life of a critical structural component, being used in an aircraft wing, Hence the estimated structural life of the whole aircraft.
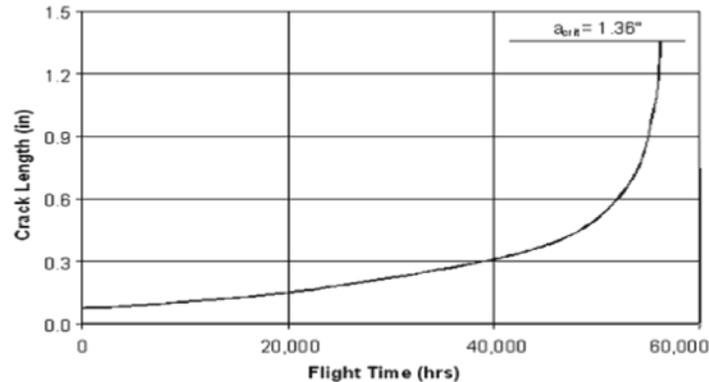
Figure 10: Resulting Graph between Crack Size and Service Life in Hours

References

[1]   http://news.bbc.co.uk/onthisday/hi/witness/october/19/newsid.stm.

[2]   Alten F Grant Jr. (2004) Fundamentals of Structural Integrity. John Wiley & Sons, Inc.Hoboken, New Jersey 12-13 .

[3]   Athena Vortex Lattice (AVL) V3.26 Software and Documentation.

[4]   http://web.mit.edu/drela/public/web/avl.

[5]   Joseph W. Cardinal and James H. Feiger (2006) Fatigue Crack Growth Equation, U.S. Department of Transportation Cambridge, MA.

[6]   Paris P. and Erdogan F. (1963) A Critical Analysis of Crack Propagation Laws, Journal of Basic Engineering, Vol. 85.

[7]   Walker K. (1970) The Effect of Stress Ratio during Crack Propagation and fatigue for 2024-T3 and 7075-T6 Aluminum, American Society for Testing and Materials, Philadelphia. PA.

[8]   NASGRO® (July 2006) Fracture Mechanics and Fatigue Crack Growth Analysis Software. v5.0, NASA-JSC and Southwest Research Institute.

[9]   James A. Harter (2006), AFGROW Users Guide and Technical Manual, Air Vehicles Directorate Air Force Research Laboratory WPAFB OH 45433USA.

[10]   G. M. Van Dijk and J.B. de Jones, (May, 1975), Introduction to FALSTAFF for Fatigue Evaluation, Structure and Material Division NLR TR 73029U.

Non-Linear Finite Element Analysis of Non-Gasketed Flange Joint under Combined Internal Pressure and Different Thermal Loading Conditions

Muhammad Abid[1], Ahsan Rauf[2] and Shahab Khushnood[3]

Abstract

Performance of a flange joint is characterized mainly due to its 'strength' and 'sealing capability'. These fundaments joints characteristics are affected in steady state and transient operating conditions. Conventional gasketed joints are prone to failure even under internal pressure loading and their performance becomes worst under applied steady state and especially at transient operating conditions. Non-gasketed joints due to the inherent static mode of load are considered as an alternative to the conventional gasketed joints for comparatively better joint strength and sealing capabilities. This paper presents the behavior of a non-gasketed bolted flanged pipe joint under bolt up, combined internal pressure, steady state and transient thermal loadings. From results flange rotation, loss in contact pressure between flange pairs, pre-load loss is observed. Based on the results, for proper joint performance, consideration of thermal loading in flange design codes is recommended. Finite element model is also verified with the available classical theories and discussed.

Keywords: Non-Gasketed Flange, Finite Element Modeling, Stress Intensity.

Introduction

The most significant contribution by Waters et al [1], for the comprehensive flange design and is the basis of well-known Taylor Forge method, BS 5500 [2], ASME VIII [3] and many other codes, do not address the effect of thermal loading on the flange joint's performance. Murray and Stuart [4] performed flange analysis for taper hub flange, removing many of the assumptions of Water's model. A number of numerical studies are available for internal pressure loading only [5, 6]. Extensive experimental studies for combined internal pressure, axial and bending loading are performed by Abid [7] to observe joint's behavior.

From these studies, failure of the gasketed flange joint is highlighted both in terms of its strength and sealing, even during bolt up conditions and becomes worst under operating conditions From this detailed study it is concluded that non-gasketed, metal-to-metal Contact joint, without a separating gasket is concluded as having 'static mode' of load due To no significant movement of the flange faces with a change in bolt up and operating conditions. Nechache et al [8] performed analytical and finite element analysis (FEA) for the determination of the steady state operating temperature profile, and the bolt load changes for the case of flange joint with a blind cover. Abid et al [9] has performed detailed FEA under steady state conditions for the non-gasketed flange joint. This paper presents detailed 2-D FEA under steady state and transient thermal loading in addition to internal pressure applied. Flange joint equivalent to 4 inch, 900 classes is used in this study.

Finite Element Modeling

In the previous work by Spence et al [11] and Abid et al [5,12], only 2-D finite element modeling and analysis is performed for internal pressure loading only. Bouzid et al [8, 13] performed FE studies using elastic material model for combined internal pressure and steady state thermal loading. In the present work, a detailed 2-D parametric FEA is performed using elasto-plastic material model for combined internal pressure, steady state and transient thermal loading. Second flange is modelled as a symmetry plate. The PLANE 82 solid structural element, PLANE 77 thermal element was used to model flange, bolt and symmetry plate. The two-dimensional 'node-to-surface' CONTA175 contact elements in combination with TARGE169 target elements were used to simulate contact distribution in analysis. 2D FE model is shown in Fig.1a, whereas steady state and thermal boundary conditions are shown in Fig. 1b & 1c. Material properties used are given in Table-1.

---

[1] Faculty of Mechanical Engineering, GIK Institute of Engineering Sciences and Technology, Topi.
[2&3] Mechanical Engineering Department, University of Engineering & Technology, Taxila.

Table 1: Allowable stresses

Parts	E (MPa)	Allowable Stress (MPa)	K (W/m-K)	α (m/m-K)	υ	ρ (kg/m³)	Cp (J/kg.k)
Flange/ Pipe[10]	203395	248	47	12.5e-6	0.3	7.86e-6	448
Bolt [10]	204000	640	37	14.1e-6	0.3	7.75e-6	486

Boundary Conditions

The flange was free to move either in axially and radial direction. Symmetric plate is constrained in both radial and axial directions. Bolt is constrained along centre nodes at the bottom surface in x direction and is free to elongate in the y-direction. Bolt Preload of 512MPa, which is 80% of the yield stress of the bolt material is applied as a bolt pre-stress value for better joint strength [5,15]. After pre-stress application, an internal pressure of 15.3MPa was applied at the inside diameter which is the design pressure for flange size of 4 inch 900# class as per code [2]. The application of the internal pressure also included the contribution of the end-cap loading. This was applied to the end of the pipe, a suitable distance away from the joint [16]. An internal fluid temperature of 1000C with convection heat transfer co-efficient of 150E-06W/mm2-k was applied on the inner surfaces of pipe and flange. Internal temperature then increased from 100-4000C. Ambient temperature was kept constant at 150C with convection heat transfer co-efficient of 20E-06W/mm2-k. [17-19]. In transient thermal analysis initial temperature of the joint was taken as 150C. Then internal fluid temperature was raised from 100-4000C with heat transfer coefficient of 150E-06W/mm2-k. Ambient temperature was kept constant with heat transfer coefficient of 20E-06W/mm2-k.The change in the temperature of the joint was calculated at each second from the start of transient to reach steady state [18].
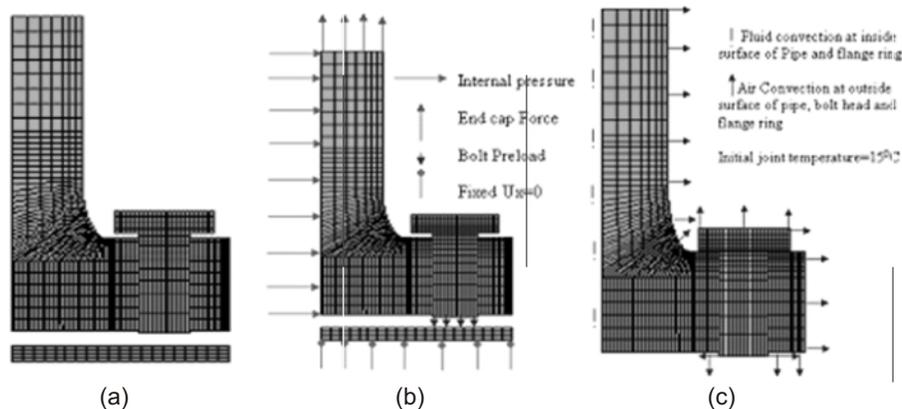

Figure 1: (a) 2-D FE Model, (b) Steady state, (c) transient thermal boundary conditions

FEA Model Verification and Results Discussion

Lame's theory [20] is used to verify the radial, tangential and longitudinal stresses in the pipe under internal pressure loading. Mathematically calculated [21] and FEA results under internal pressure, steady state and thermal loading at pipe section are found in good agreement [Fig. 2a,b]. Time required reaching for the joint to reach in steady state at the outside surface of the pipe is calculated mathematically.

Flange Stress Intensity (SINT)

Stress intensity in the flange under bolt up, internal pressure and different thermal loading is shown in Fig. 4. Flange is observed relaxed more at the start of the transient process as compared to when it reached the steady state. Flange relaxed 5% more at 76 seconds at 1000C, 15% more at112 seconds at 2000C and 15% more at 124 seconds at steady state temperature.
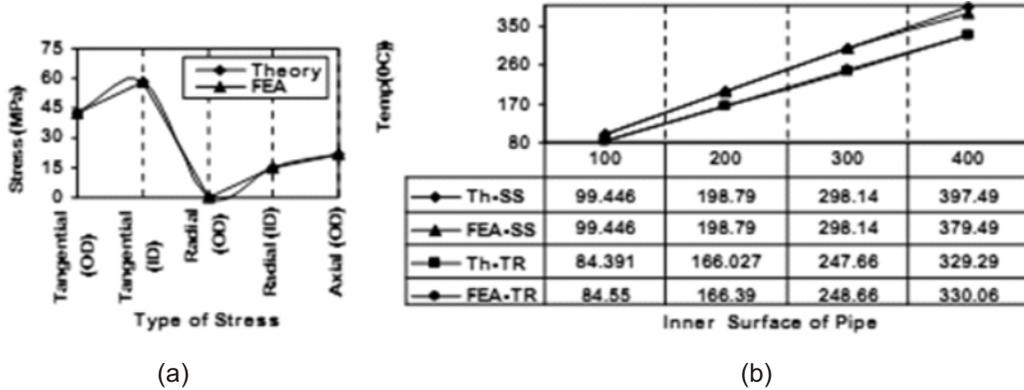
Figure 2: FEA model verification for; (a) Stresses, (b) Temperature at pipe inside diameter under steady state and transient loading (Th-Theory, SS-Steady state, TR-Transient)
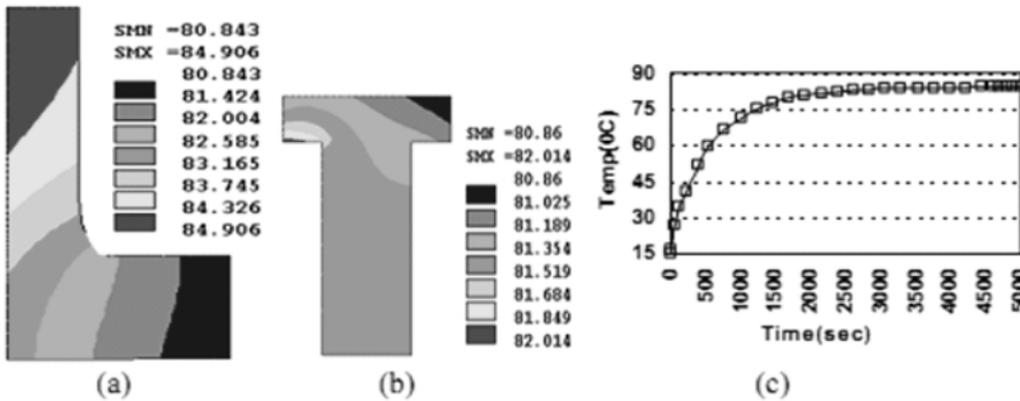
Figure 3: Temperature distribution at 100oC in (a) Flange, (b) Bolt and (c) Transient temperature variation at outside surface of pipe with time
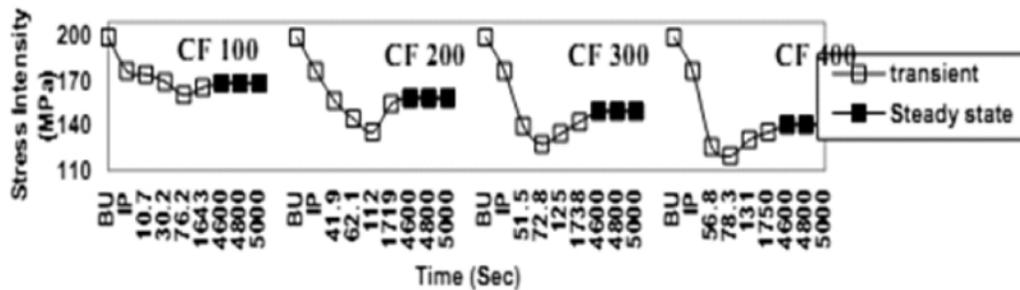
Figure 4: Max. SINT variation in flange with time

Bolt Stress Intensity (SINT)

SINT in the bolt increased in the early transient of steady state. At bolt up SINT in the bolt was (556 MPa) that further increased to (559 MPa, 560 MPa and 562 MPa) at 35% (i.e. at 76,112,124 Sec) of steady state temperature 1000C, 2000C and 3000C respectively. This increase at 35% of steady state temperature shows that it requires time some for heat to reach in the bolt. Flange expanded at this time of temperature loading and bolt does not expand that ultimately increases the load on the bolt.

Contact pressure variation at flange inside diameter

Contact pressure at the inside diameter of the flange ring is decreased under internal pressure loading [Fig. 6] and then slightly increased at the initial transients and finally again decreased at the steady state condition. This relaxation in contact pressure at the inside diameter can result in the possible leak from the joint.

Figure 6: Contact pressure variations at flange inside diameter with time

Axial flange displacement at inside diameter

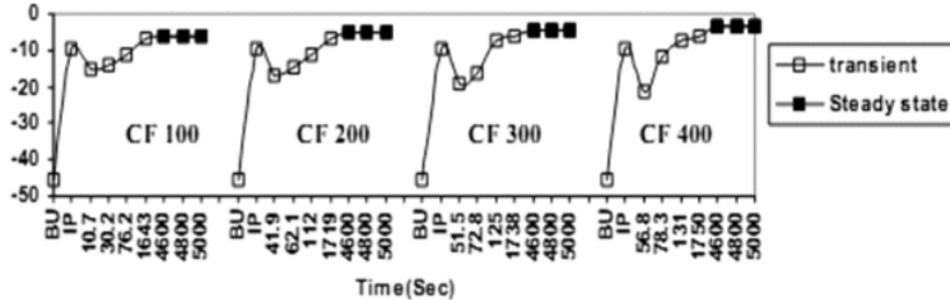Internal pressure tends to separate the contact nodes between the flange pairs at inside diameter [Fig. 7]. At the initial transients the gap tends to close at the contact nodes at inside diameter. As soon as the joint reach steady state, the contact nodes again tend to separate. Increased in fluid temperature tends to open the gap more after reaching in steady state.
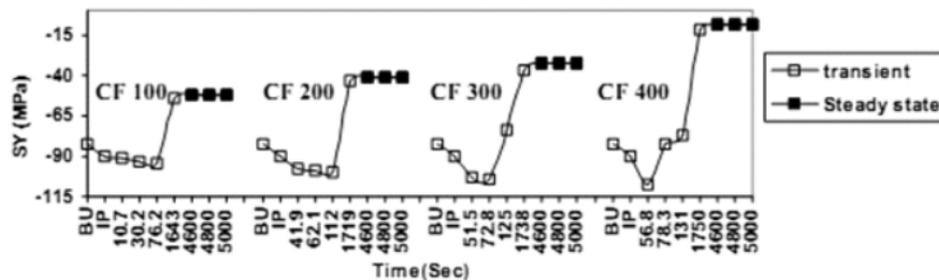

Figure 7: Axial flange displacement at inside diameter with time

Fundamental Joint Characteristics

In this section, behavior of non-gasketed bolted flanged pipe joint under steady state and transient thermal loading is discussed. Specific emphasis is given to the strength and to the possible sealing characteristics of the joint. Correct functioning of a flanged joint is given if it is tight, and its integrity is guaranteed for the entire period of operations. Integrity is achieved by limiting the stress in the component and tightness means that the joint remains within its Tightness class under all states of operations, i.e. the leak rates are within the specified limits. Sealing ability can not be determined directly from this finite element work since no direct correlation to leakage has been made by the present author. However Abid [22] during his work for leakage provided this direct correlation using experimentental study and has concluded that leakage is directly proportional to the gap at the inside diameter of flange. Hence, any comments about the sealing ability of the flanged joint will be based upon the contact pressure and initial gap at inside diameter of the flange. For accurate prediction of the leakage behavior, further experimental work is obviously required to determine the relation ship of contact pressure and the sealing ability of the joint.

Joint Strength

At maximum allowable working pressure of 15.3MPa, the maximum stress intensity in the flange is less than the allowable stress of the flange material. The stress is higher at the hub flange fillet. A higher stress is

also observed at the area under the bolt head, due to high applied preload in the bolt. The rotation of the joint from inside to outside diameter is almost negligible at the allowable working pressure. There is high stress at the top of the bolt shaft close to the bolt head and shank corner. However no yielding is observed and the maximum stress in the bolt is less than the allowable stress of the bolt material. There is small increase of bending stress in the bolt when the joint is subjected to transient thermal loadings. This increase in the bending stress is observed when the joint comes in operation after installation. No yielding is observed in the joint components in operating conditions, so joint is concluded safe.

Sealing Capability

The sealing of joints is measured from the contact pressure variation between the flanges faces under all the applied loading conditions. After bolt up, two surfaces of the flange pairs compress each other. This contact pressure is essential for the sealing of the joint. The application of internal pressure and addition thermal loading tends to decrease the contact pressure between the flange pairs. After the installation of joint the initial transient's increases the contact pressure but when the joint reach its steady state, contact become loosen and can result in possible leakage.

Conclusions

It is concluded that the non-gasketed joint has structural integrity under applied operating conditions. But the sealing capability of the joint is affected with thermal loads. These thermal loads tend to relax the joint. The sealing capability of the joint is related to the contact pressure between the flange faces. Early transition of thermal loadings relaxed the flange more as compared to steady state thermal loading. It also increased the load on the bolt. It is concluded from transient analysis that the joint is safe from leakage in early transit but prone to leakage as the joint tend to attain steady state.

References

[1]   Waters, E. O., Wesstrom, D. B., Rossheim, D. B., and Williams, F. S. G. 1937. "Formulas for Stresses in Bolted Flanged Connections". Transactions of ASME,   59, 161.

[2]   BS 5500.1991"Unfired Fusion Welded Pressure Vessels". British StandardsInstitution, London, UK.

[3]   ASME Boiler and Pressure Vessel Code, Section VIII", 1998. American Society ofMech. Eng., New York, USA.

[4]   Murray, N. W. and Stuart, D. G. 1961. "Behavior of Large Taper Hub Flanges. Proc. Symp.Pressure Vessel Research towards Better Design", Institute of Mechanical Engineers, 133.

[5]   Abid, M., Nash, D. H. 2004. "Comparative study of the behaviour of conventional gasketed and compact non-gasketed flanged pipe joints under bolt up and operating conditions". International Journal of Pressure Vessels and Piping, 80, 831-841.

[6]   Power, D. J. (1997). A Study of Conventional and Unconventional Flanged Pipe Joint Styles   Using Non Linear Finite Element Analysis Techniques. M.Phil. Thesis.

[7]   Abid, M. (2000). Experimental and Analytical studies of conventional (gasketed) and unconventional (non gasketed) flanged pipe joints (with special emphasis on the engineering of 'joint strength' and 'sealing') PhD Thesis.

[8]   Nechache A., Bouzid A H., Brown W., 2002 'The effect of Steady State Thermal Loading on the Deflection of a Flanged Joint with a Cover Plate', ASME Pressure Vessel and Piping PVP, 2002, Conference, Vancouver, British Columbia, Canada.

[9]   Muhammad Abid, "Determination of safe operating conditions for non-gasketed flange joint   under combined internal pressure and temperature" International Journal of Mechanics and Materials in Design by Springer. DOI 10.1007/s10999-005-4447-2. (2005) 2: 129-140.

[10]   "ASME Boiler and Pressure Vessel Code, Section II, Part D", 1998. American Society of Mech. Eng., New York, USA.

[11]   Spence, J., Macfarlane, D. M. and Tooth, A. S. 1998. "Metal-to-Metal full face taper hub flanges: finite element model evaluation and preliminary plastic analysis". Proc.

Instn. Mech. Engrs. 212 (E), 57-69.

[12]   Nash, D. H., Spence, J., Tooth, A. S., Abid, M., and Power, D. J. 2000. "A parametric study of metal-to-metal full faces taper hub flanges". Intl. Journal of Pressure Vessels and Piping, 77 (13), 791-798.

[13]   Bouzid, A. and Nechache, A. 2002. "The Effect of Steady State Thermal Loading on the Deflections of Flanged Joint with a Cover Plate". ASME Intl. PVP Conference, USA, 433, 153-162.

[14]   ANSYS Inc., 2006 ANSYS Elements Manual, Seventh Edition.

[15]   Webjörn J., 1967, 'Flange Design in Sweden', Proceedings of the Petrochemical Mechanical Engineering Conference, American Society of Mechanical Engineers, Philadelphia PA, September 17-20 1967. Paper 67-PET-20.

[16]   Thomson G., 1988 'Strength and Flexibility of Pressurized Taper Hub Flanged Joints', Applied Solid Mechanics - 2, Editors, Tooth, A. S., and Spence, J., Ch. 13, Elsevier Applied Science Publications, London.

[17]   Bouzid A., Nechache A., 2005 'thermally induced deflections in bolted flanged connections'. Transactions of the ASME 394/Vol.127.

[18]   Sawa T., Hirose T., Nakagomi Y., 1996 'Behavior of a tapered hub flange with a bolted flat cover in transient temperature field', Journal of pressure vessel technology, Vol.118/115.

[19]   Alghamdi A., Al-sannaa., 2004 'Two dimensional finite element analysis for large diameter steel flanges'. Journal of pressure vessel technology, august 2004, Vol 126/39 9.

[20]   John F. Harvey, P.E. 'Theory and Design of Pressure Vessels', CBS Publishers.

[21]   Holman, J.P. 1986. H eat and Mass Transfer. ISBN 0-07-029620-0.

[22]   Nash D H., Spence J., Tooth A S., Abid M., Power D J., 2000 "A parametric study of metal-to-metal full face taper-hub flanges", The Ninth International Conference on Pressure Vessel Technology; ICPVT-9, Sydney.

Guidelines And Information For Authors

General

Papers may be submitted any time throughout the year. After having received a paper it is sent to three referees, at least one from a technology advanced countries. Papers reviewed and declared fit for publication before 31 December are published next year before 31 March every year. Papers must be submitted on a CD with FOUR Hard copies to the editor Technical journal, University of Engineering and Technology Taxila. Soft copy by e-mail to the following address is preferred:

technical.journal@uettaxila.edu.pk

Authors are required to read the following carefully for writing a paper.

Text

Text should be type-written with M.S word, Arial Font size 10.at single space and with margins as 1.5 inch top, 1 inch right, 1 inch left and 1 inch bottom, on an A-4 size, paper. The title page should include; the title; the name/names of the authors and their addresses, an abstract of about 200 words and keywords followed by the introduction. The text of the paper may be divided into introduction, methodology/Analysis results and discussion, conclusion, references and acknowledgment (if any). All pages should consist of single columns text.

Length

Research paper should not exceed 15 pages as per specifications given above.

Elements of Paper

The basic elements of paper are listed below in the order in which they appear: Title, names of the author and affiliations, Abstract, Body of paper, Acknowledgments, Nomenclature, references, Appendices.

Title

The title of the paper should be concise and definitive.

Names of Authors and Affiliations

Names of authors should consist of first name (or initial), middle initial and last name. The author affiliation should consist of his full address.

Abstract

An abstract up to a maximum of 200 words should open the paper. The abstract should give a clear indication of the objectives, scope and results, the abstract text may be organized to include the background, methods, results and conclusions.

Keywords

Keywords should be included on a separate line at the end of the abstract.

Body of the Paper

Body of the paper may include introduction and literature review, materials and methods, modeling/experimentation, results-discussions and conclusions.

Originality

Only original contributions to engineering and Science literature should be submitted for publication. It should incorporate substantial information not previously published.

Accuracy

All the technical, scientific and mathematical information contained in the paper should be checked with great care.

Use of SI Units

Preferably SI units of Measurements be included.

Mathematics

Equations should be numbered consecutively beginning with (1) to the end of the paper. The number should be enclosed in parentheses (as shown above) and set flush right in the column on the same line as the equation. This number then should be used for referring the equation within the text. Equation may be referenced within the text as "E q. (x)"."When the reference to an equation begins a sentence, it should be spelled out fully, as "Equation (x).in all mathematical expressions and analyses, symbols (and the units in which they are measured) not previously defined in nomenclature should be explained.

Figures

All figures (graphs, line drawings, photographs, etc.) should be numbered consecutively and have a caption consisting of the figure number and a brief title or description of the figure. This number should be used when referring to the figure in the text. Figure references should be included within the text in numerical order according to their order of appearance. Figure may be referenced within the text as "Fig.-x". When the reference to a figure begins a sentence, the abbreviation "Fig," should be spelled out e.g.," Figure-x"

Tables

All tables should be numbered consecutively. Tables should have a caption consisting of the table number and brief title. This number should be used when referring to the table in text. Table references should be included within the text in numerical order according to their order of appearance. Table should be inserted as part of the text as close as possible to its first reference.

Acknowledgments

All individuals or institutions not mentioned elsewhere in the work who have made an important contribution should be acknowledged.

References

Within the text, references should be cited with name of the author and year in parenthesis. The reference list will be arranged alphabetically.

Example

Chamber (1959) has described a method and Wormleaton (2006) used this method. In case of two authors, name of both the authors will appear with year. For example Khan and Ghumman (2008) studied hydrodynamic modeling for water-saving strategies in irrigation canals. In case of three or more authors it will be cited as: Ghumman et al. investigated use of numerical modeling for management of canal irrigation water in case of continuous references, the references may be separated by comma"," See the list of sample references.

List of References

References to original source of the cited material as given above as sample reference should be listed together at the end of the paper, footnotes should not be used for this purpose. References should be arranged in alphabetic order. Each reference should include the last name of each author followed by his initials.

1. Reference to journal articles and paper in serial publication include :Last name of each author followed by their initial, Year of publication, Full title of the cited article, Full name of the publication in which it appears, Volume number (if any) in boldface, Issue number (if any) in parentheses, Inclusive page number of the cited article.

2. Reference to the text books and monographs should include: Last name of each author followed by their initial, Year of publication, Full title of the publication, Publisher, City of publication, Inclusive page number of the work being cited, Chapter number(if any).

3. Reference to original conference papers, papers in compiled conference proceedings or any other collection of woks by numerous authors should include: Last name of each author followed by their initial, Year of publication, Full title of the cited paper in quotes, individual paper number (if any) ,Full title of the publication , Initial followed by the name of the editor (if any),followed by the abbreviation, "eds" ,Publisher, City of publication, Volume number (if any),Inclusive Page number of the work being cited.

4. Reference to thesis and technical reports should include: Last name of each author followed by their initial, Year of publication, Full title in quotes, title capitalization, Report number(if any) Publisher or the institution name, City.

Sample References

[1]   Bievere B.D Alvarado, A.Timbe, L. Celleri and J. Feyen 2003.Night irrigation reduction for water saving in medium-sized system, Journal of irrigation and Drainage Engineering, ASCE   Vol.129, N0.2.337-348.

[2]   Chamber R.1988. Managing canal irrigation: Practical Analysis from South Asia, Institution of Development Studies, Oxford & IBH Publishing Co. Ltd.

[3]   Strelkof T.1969.One-dimentional equations of open-channel flow. J. Hydraulics Div., ASCE, Vol.95 (HY3):861-876

[4]   Khan,M.Z. 2006. Investigation of the optimal operation strategies for irrigation systems. Ph.D.Dissertation. Department of Civil Engineering, University of Engineering and Technology Taxila.

[5]   Ghumman, A.R., M.Z. Khan, and M.J. Khan.2006.Use of numerical Modeling for Management of Canal Irrigation Water. Irrigation and Drainage.Wilay Intersciencez. : 445-458.

[6]   Khan M. Z. and Ghumman A. R.2008, Hydrodynamic Modeling For Water-Saving Strategies In Irrigation Canals.